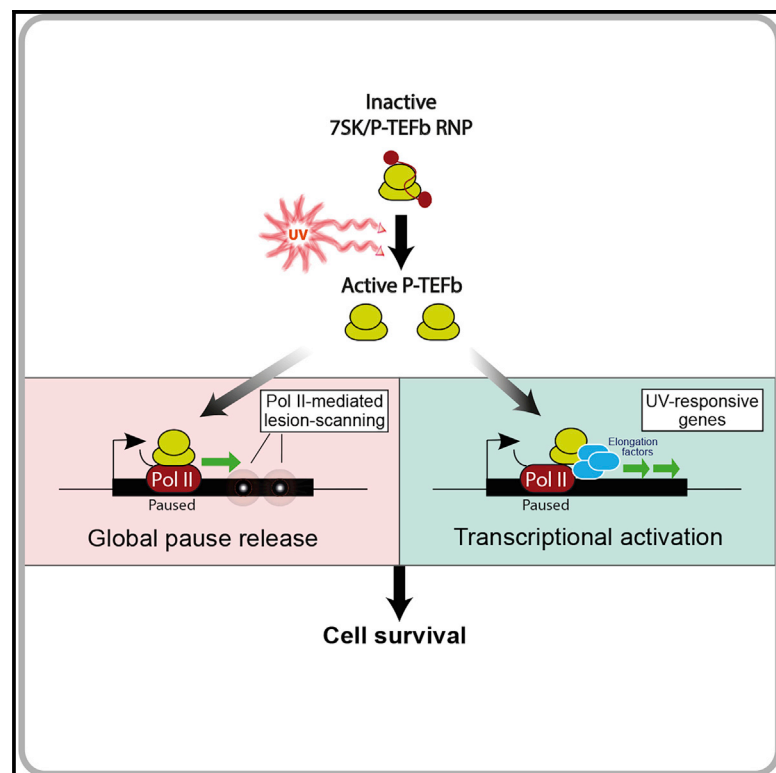


The 7SK/P-TEFb snRNP controls ultraviolet radiation-induced transcriptional reprogramming

Graphical abstract



Authors

Cécilia Studniarek, Michael Tellier, Pascal G.P. Martin, Shona Murphy, Tamás Kiss, Sylvain Egloff

Correspondence

tamas.kiss@univ-tlse3.fr (T.K.),
sylvain.egloff@univ-tlse3.fr (S.E.)

In brief

Studniarek et al. demonstrate that under UV-induced stress conditions, human cells lacking the 7SK/P-TEFb regulatory snRNP show compromised transcriptional response and reduced cell viability. The 7SK/P-TEFb snRNP provides active P-TEFb to promote the genome-wide release of promoter-proximally paused RNAPII and to stimulate productive elongation on hundreds of important UV-responsive genes.

Highlights

- The 7SK snRNA is dispensable for cell proliferation under standard growth conditions
- After UV exposure, 7SK/P-TEFb is needed for proper stress response and cell survival
- P-TEFb extracted from 7SK/P-TEFb triggers UV-induced general RNAPII pause release
- P-TEFb from 7SK/P-TEFb supports activation of important UV-responsive genes



Article

The 7SK/P-TEFb snRNP controls ultraviolet radiation-induced transcriptional reprogramming

Cécilia Studniarek,¹ Michael Tellier,² Pascal G.P. Martin,³ Shona Murphy,² Tamás Kiss,^{1,4,*} and Sylvain Egloff^{1,5,*}¹Molecular, Cellular and Developmental Biology Department (MCD), Centre de Biologie Intégrative (CBI), University of Toulouse, CNRS, UPS, 31062 Toulouse, France²Sir William Dunn School of Pathology, University of Oxford, Oxford OX1 3RE, UK³INRA UMR1331, ToxAlim, Toulouse, France⁴Biological Research Centre, Szeged, Hungary⁵Lead contact*Correspondence: tamas.kiss@univ-tlse3.fr (T.K.), sylvain.egloff@univ-tlse3.fr (S.E.)<https://doi.org/10.1016/j.celrep.2021.108965>

SUMMARY

Conversion of promoter-proximally paused RNA polymerase II (RNAPII) into elongating polymerase by the positive transcription elongation factor b (P-TEFb) is a central regulatory step of mRNA synthesis. The activity of P-TEFb is controlled mainly by the 7SK small nuclear ribonucleoprotein (snRNP), which sequesters active P-TEFb into inactive 7SK/P-TEFb snRNP. Here we demonstrate that under normal culture conditions, the lack of 7SK snRNP has only minor impacts on global RNAPII transcription without detectable consequences on cell proliferation. However, upon ultraviolet (UV)-light-induced DNA damage, cells lacking 7SK have a defective transcriptional response and reduced viability. Both UV-induced release of “lesion-scanning” polymerases and activation of key early-responsive genes are compromised in the absence of 7SK. Proper induction of 7SK-dependent UV-responsive genes requires P-TEFb activity directly mobilized from the nucleoplasmic 7SK/P-TEFb snRNP. Our data demonstrate that the primary function of the 7SK/P-TEFb snRNP is to orchestrate the proper transcriptional response to stress.

INTRODUCTION

Promoter-proximal pausing is a key regulatory step in the expression of most RNA polymerase II (RNAPII)-transcribed genes (Core and Adelman, 2019; Jonkers and Lis, 2015; Zhou et al., 2012). RNAPII pausing is particularly prominent on stimulus-induced, developmentally regulated, and signaling pathway genes (Adelman and Lis, 2012; Williams et al., 2015). After transcription initiation, the negative elongation factor (NELF) and the 5,6-dichlorobenzimidazole-1- β -D-ribofuranoside (DRB)-sensitivity-inducing factor (DSIF) bind to RNAPII to block its progression. To release paused RNAPII and to support productive elongation, positive transcription elongation factor b (P-TEFb), a cyclin (Cyc)-dependent protein kinase composed of Cdk9 and Cyc T1 or T2, phosphorylates NELF, the Spt5 subunit of DSIF, and the C-terminal domain (CTD) of RNAPII at Ser2 (Gressel et al., 2017; Jonkers et al., 2014; Peterlin and Price, 2006; Price, 2000). The phosphorylated NELF-P dissociates from RNAPII, DSIF-P functions as an elongation stimulating factor, and Ser2-P promotes co-transcriptional splicing and 3' end processing of the nascent pre-mRNA (Peterlin and Price 2006; Zhou et al., 2012). Releasing paused RNAPII is now recognized as a central determinant of eukaryotic gene expression (Jonkers and Lis, 2015; Quaresma et al., 2016; Smith and Shilatifard, 2013; Zhou et al., 2012).

The nuclear activity of P-TEFb is controlled mainly by the 7SK small nuclear ribonucleoprotein (snRNP) composed of the 7SK small nuclear RNA (snRNA), the La-related protein 7 (Larp7), and the methylphosphate capping enzyme (MePCE) (Jerónimo et al., 2007; Krueger et al., 2008). Together with the hexamethylene bisacetamide-inducible proteins 1 and 2 (HEXIM1/2), the 7SK snRNP sequesters P-TEFb into a large kinase-inactive 7SK/HEXIM/P-TEFb complex, hereafter called the 7SK/P-TEFb snRNP (Nguyen et al., 2001; Yang et al., 2001). HEXIM1/2 binds to and inhibits the kinase activity of P-TEFb in a 7SK-dependent manner (Kobbi et al., 2016; Michels et al., 2004). Some environmental conditions and signaling pathways trigger 7SK/P-TEFb dissociation to increase the level of active P-TEFb available for transcription stimulation (Quaresma et al., 2016). Thus, the 7SK/P-TEFb snRNP represents an important P-TEFb reservoir from which active P-TEFb can be rapidly mobilized in response to transcriptional stimuli (Zhou et al., 2012).

P-TEFb recruitment to transcriptionally active genes is directed by diverse transcription factors and RNA binding proteins, including the BET bromodomain protein Brd4 (Jang et al., 2005; Quaresma et al., 2016; Yang et al., 2005). Another fraction of P-TEFb associates with the super elongation complexes (SECs), which contain additional elongation factors, such as ELL, and stimulate RNAPII processivity very efficiently



(He et al., 2010; Lin et al., 2010; Luo et al., 2012; Sobhian et al., 2010; Yokoyama et al., 2010; Zhou et al., 2012). Recent studies proposed that the 7SK/P-TEFb snRNP can be loaded onto selected promoters where active P-TEFb is locally extracted and used for RNAPII pause release (D'Orso and Frankel, 2010; McNamara et al., 2013, 2016). Genome-wide analyses reported enrichment of 7SK snRNP components at the promoter regions of most human protein-coding genes, arguing for prevalent 7SK/P-TEFb anchoring to chromatin (Calo et al., 2015; Ji et al., 2013; McNamara et al., 2016). Coordinated 7SK/P-TEFb loading onto selected promoters might stimulate rapid and synchronous transcriptional activation in response to environmental cues (Bugai et al., 2019; McNamara et al., 2013).

Exposure to ultraviolet (UV) light provokes rapid release of P-TEFb from the 7SK/P-TEFb snRNP and also induces profound transcriptional reprogramming, with most genes being repressed while early UV-response genes are activated (Bugai et al., 2019; Zhou et al., 2012; Zhou and Yik, 2006). In addition, UV-induced DNA damage provokes a global release of promoter-proximally paused RNAPII (Lavigne et al., 2017). The UV-released polymerases display low elongation rates, and their transcriptional range is restricted to 25 kb (Williamson et al., 2017). This wave of elongating polymerases is thought to allow rapid and efficient lesion detection by the transcription machinery and to facilitate DNA repair by the transcription-coupled nucleotide excision repair (TC-NER) pathway. It is unknown whether 7SK/P-TEFb dissociation, either in the nucleoplasm or on the chromatin, is directly involved in the UV-induced transcriptional response.

To further investigate the transcriptional regulatory function of the 7SK/P-TEFb snRNP, we generated a human 7SK knockout (KO) cell line that accumulates only the active form of P-TEFb and lacks the ability to rapidly augment P-TEFb activity and to load 7SK/P-TEFb onto the chromatin. Under normal growth conditions, the 7SK KO cells show minor changes to genome-wide RNAPII transcription, including reduced promoter-proximal pausing, without detectable consequences on cell proliferation. However, after UV irradiation, the 7SK KO cells show highly reduced viability, probably because they are unable to orchestrate a proper transcriptional response to UV-induced DNA damage. The lack of 7SK impairs both UV-triggered release of "lesion-scanning" polymerases and activation of a set of important early-responsive genes. We demonstrate that correct activation of 7SK-dependent UV-induced genes cannot be ensured by free P-TEFb, and it requires the 7SK/P-TEFb snRNP. Mechanistically, P-TEFb directly extracted from 7SK/P-TEFb and incorporated into SECs is loaded onto UV-induced genes to stimulate RNAPII release and recruitment of RNAPII elongation factors.

RESULTS

Human cells lacking 7SK snRNA retain normal growth properties

Expression of the RNAPIII-transcribed human gene for 7SK snRNA (7SK) is governed by upstream promoter elements, the TATA-box and the proximal and distal sequence elements (PSEs and DSEs) (Figure S1A; Diribarne and Bensaude, 2009). To abrogate 7SK snRNA production in human HAP1 cells, we

disrupted the essential PSE promoter element of the 7SK gene by CRISPR-Cas9 genome editing. Northern blot analysis and fluorescence *in situ* hybridization demonstrated that targeted PSE destruction fully abolished 7SK accumulation (Figure 1A; Figure S1A). To exclude potential CRISPR-Cas9 off-target effects, we rescued 7SK expression in our 7SK KO cells through stable re-insertion of the full-length 7SK gene, restoring about 60%–70% of the 7SK snRNA level observed in HAP1 cells (Figure 1A, 7SK RST). As controls, two additional 7SK-deficient HAP1 cell lines were generated with excision of the entire 7SK coding region (7SKex KO; Figure S1B) and disruption of *Larp7* expression that also abolished 7SK accumulation (*Larp7* KO; Figure S1C).

To characterize P-TEFb-containing complexes in HAP1, 7SK KO, and 7SK RST cells, we size-fractionated cell lysates by velocity sedimentation through glycerol gradients, and distribution of the 7SK snRNP (MePCE and *Larp7*), P-TEFb (Cdk9 and Cyc T1), and HEXIM1 was monitored by western blot analysis (Figure 1B). In HAP1 cells, about half of Cdk9 and Cyc T1 and a small portion (~5%–10%) of HEXIM1 were found in fractions 6 and 7 containing the large 7SK/P-TEFb snRNP (large complex [LC]) (Nguyen et al., 2001; Yang et al., 2001). The other half of Cdk9 and Cyc T1, which corresponds to free P-TEFb, was detected in fractions 3 and 4 (small complex [SC]). As expected, most of MePCE and a great portion of *Larp7* co-sedimented with the large 7SK/P-TEFb complex (Krueger et al., 2008). In 7SK KO cells, all 7SK-associated proteins, Cdk9, Cyc T1, HEXIM1, MePCE, and *Larp7*, were shifted from the LC fractions toward lighter fractions, consistent with the idea that the 7SK RNA provides the scaffold for 7SK/P-TEFb assembly. Importantly, the wild-type sedimentation properties of all 7SK proteins and the 7SK snRNA were restored in 7SK RST cells (see also Figure S1D). The sedimentation profile of hnRNP A1 was not detectably affected by 7SK loss because only a small fraction of hnRNP A1 binds to 7SK (Barrandon et al., 2007; Van Herreweghe et al., 2007).

Co-immunoprecipitation confirmed that the protein-protein interactions supporting HAP1 7SK/P-TEFb assembly are lost in 7SK KO and are reestablished in 7SK RST cells (Figure 1C). In the absence of 7SK, the interaction of HEXIM1 with P-TEFb, MePCE, and *Larp7* is fully abolished, confirming the 7SK dependency of HEXIM1-mediated P-TEFb inhibition (lane 8). Co-precipitation of Cyc T1 and Cdk9 confirms that 7SK KO cells express only the active form of P-TEFb and lack 7SK- and HEXIM1-associated inactive P-TEFb (lanes 11 and 14).

Disruption of 7SK expression was expected to augment P-TEFb activity and to promote cell proliferation (He et al., 2008). However, cell counting and MTS cell proliferation assays failed to detect growth anomalies for 7SK KO cells (Figure 1D; Figure S1E). Measuring global RNA synthesis by ethynyl uridine (EU) incorporation assays showed that the transcription rate does not vary significantly between HAP1 and 7SK KO cells (Figure S1F). Consistently, western analyses showed that the phosphorylation state of RNAPII CTD, including CDK9-mediated Ser2 phosphorylation, is not affected by the absence of 7SK (Figure S1G). In contrast, we noticed that accumulation of both Cdk9 and Cyc T1 was significantly reduced in the 7SK-deficient 7SK, 7SKex, and *Larp7* KO cells (Figure 1A; Figures S1B and S1C). Importantly, restoration of 7SK expression reestablished

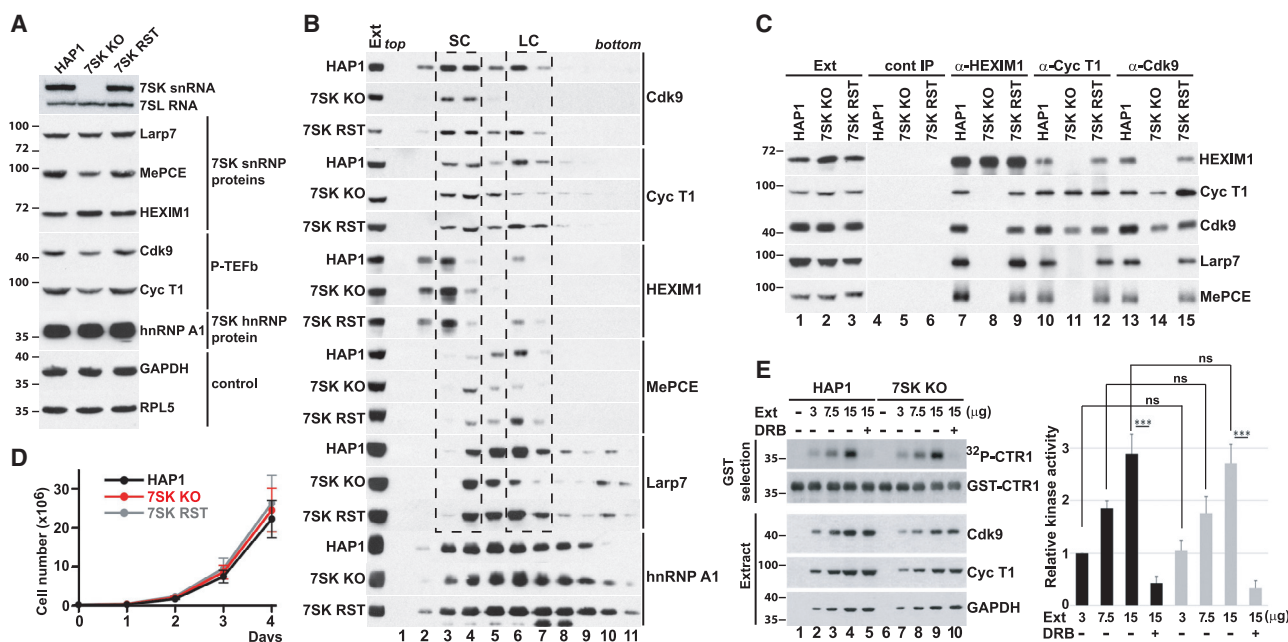


Figure 1. Characterization of human HAP1 7SK knockout (KO) cells

(A) Total extracts and RNAs from HAP1, 7SK KO, and 7SK-restored (RST) cells were analyzed by western and northern blotting. (B) Sedimentation analysis of P-TEFb complexes. Extracts (Ext) from HAP1, 7SK KO, and 7SK RST cells were fractionated by centrifugation on a 10%–40% glycerol gradient. The gradient was divided into 12 fractions, and distribution of Cdk9, Cyc T1, HEXIM1, MePCE, Larp7, and hnRNP A1 was monitored by western blotting. Fractions containing the small P-TEFb (SC) and the large 7SK/P-TEFb (LC) complexes are indicated. (C) Interaction of 7SK/P-TEFb snRNP proteins. From HAP1, 7SK KO, and 7SK RST cell extracts, co-immunoprecipitation of endogenous HEXIM1, Cyc T1, and Cdk9 with other components of the 7SK/P-TEFb snRNP was tested by western blotting. (D) Proliferation rates of HAP1, 7SK KO, and 7SK RST cells under normal growth conditions. Error bars represent standard deviations from three independent experiments. (E) *In vitro* Cdk9 kinase assay. In the presence of γ -³²P-ATP, recombinant GST-CTR1 was incubated with or without the indicated amounts of Ext prepared from DRB-treated or non-treated HAP1 and 7SK KO cells. The purified GST-CTR1 and endogenous Cdk9, Cyc T1, and GAPDH levels were monitored by western blotting. CTR1 phosphorylation was measured by autoradiography and quantitated by phosphorimager in at least three independent experiments. ***p < 0.001, determined by Student's t test. ns, not significant. See also Figure S1.

the wild-type level of P-TEFb accumulation in 7SK RST cells, demonstrating that downregulation of P-TEFb is linked to the intracellular level of 7SK snRNA (Figure 1A). Consistent with previous observations that 7SK/P-TEFb disruption upregulates HEXIM1 expression (Castello-Brancato et al., 2013; Liu et al., 2014), our 7SK and Larp7 KO cells also showed increased HEXIM1 accumulation (Figure 1A; Figure S1C). We propose that in the prolonged absence of 7SK snRNP, compensatory mechanisms prevent P-TEFb over-activation and uncontrolled cell proliferation through reducing Cdk9 and Cyc T1 accumulation. Maintaining P-TEFb activity at normal levels may therefore be critical for survival of human cells.

Human P-TEFb phosphorylates the C-terminal repeat 1 (CTR1) of Spt5 at Thr806 to potentiate the elongation stimulatory activity of DSIF (Larochelle et al., 2006; Parua et al., 2018; Sansó et al., 2016; Yamada et al., 2006). To compare Cdk9 activities in HAP1 and 7SK KO cells, we incubated extracts from both cell lines with glutathione S-transferase (GST)-fused recombinant Spt5 CTR1 (amino acids [aa] 720–830) in the presence of γ -P³²ATP (Larochelle et al., 2006). The *in vitro* phosphorylation of CTR1 was measured by autoradiography following GST-CTR1 purification on glutathione resin (Figure 1E). Despite the

reduced global P-TEFb level in 7SK KO cells, the two extracts showed similar CTR1-specific kinase activities, indicating that HAP1 and 7SK KO cells contain comparable levels of active P-TEFb. Importantly, CTR1 phosphorylation was largely inhibited by pre-treatment of the cells with Cdk9 inhibitors such as DRB or FP (flavopiridol), confirming that CTR1 phosphorylation was P-TEFb dependent (Figure 1E; Figure S1H). We concluded that after 7SK depletion, the 7SK-associated fraction of P-TEFb disappears; therefore, the parental HAP and the resulting 7SK KO cells contain similar levels of active P-TEFb.

Lack of 7SK affects RNAPII transcription and promoter-proximal pausing

Because P-TEFb regulates productive elongation, we compared RNAPII transcription dynamics and pausing in HAP1 and 7SK KO cells. We determined the genome-wide occupancy of transcriptionally engaged RNAPII by mammalian native elongating transcript sequencing (mNET-seq) (Nojima et al., 2015, 2016). Spearman correlations of independent biological replicates showed highly reproducible signals for each tested condition ($\rho \geq 0.8$; Figure S2A). Based on reported RNA sequencing (RNA-seq) data, we divided HAP1 protein-coding genes into

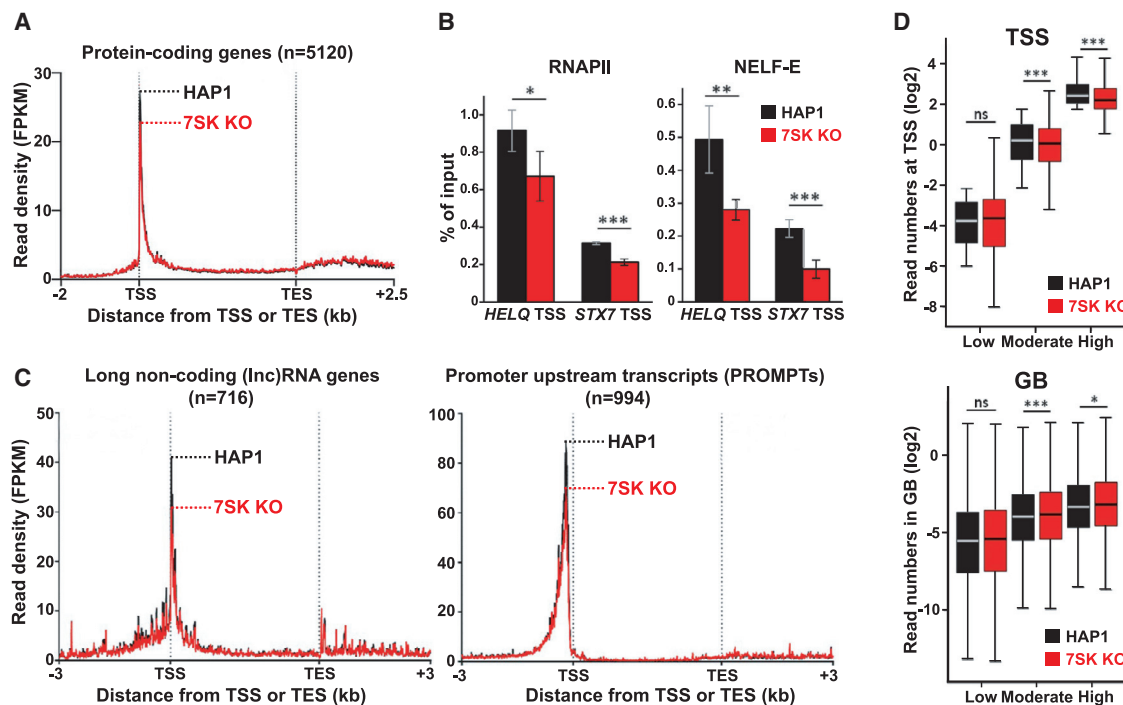


Figure 2. Decreased promoter-proximal pausing in 7SK KO cells

(A) Meta-analysis of mNET-seq over protein-coding genes in HAP1 and 7SK KO cells. Horizontal dotted lines indicate the average level of RNAPII promoter-proximal pausing.

(B) Quantitative ChIP analyses of endogenous RNAPII and NELF-E occupancy at the TSS of *HELQ* and *STX7* genes in HAP1 and 7SK KO cells. * $p < 0.05$; ** $p < 0.01$; *** $p < 0.001$, determined by Student's *t* test.

(C) Meta-analysis of mNET-seq over lncRNA genes and PROMPTs (negative strands) in HAP1 and 7SK KO cells.

(D) Boxplot presentation of the quantification of mNET-seq reads at TSS (top panel) and in gene bodies (GBs) (bottom panel) in HAP1 and 7SK KO cells. Genes were sorted into three equal groups characterized by low, moderate, and high red numbers at their TSS in HAP1 cells. Genes with higher TSS read density showed larger reduction in promoter-proximal pausing in 7SK KO cells. * $p < 0.05$; *** $p < 0.001$, determined by Wilcoxon test.

See also Figure S3.

four quartiles (Q1–Q4) with increasing expression levels (Rodríguez-Castañeda et al., 2018). Good correlation was observed between the RNA-seq and mNET-seq signals. Namely, the highly expressed genes displayed higher mNET-seq signals both at the promoter-proximal region (from transcription start site [TSS] to +250 bp) and in the gene body (GB) (from +250 bp to transcription end site [TES]) (Figures S2B and S2C). Quantification of mNET-seq reads in GBs was used to compare the transcription levels in HAP1 and 7SK KO cells. This approach detected 1,592 upregulated and 992 downregulated genes in 7SK KO cells (fold-change induction [FC] ≥ 1.5 ; see Figure S2D for Gene Ontology [GO] enrichment analysis). The upregulated genes showed increased RNAPII occupancy at both TSS and GB in 7SK KO cells, while the downregulated ones exhibited decreased occupancy (Figures S2E and S2F). Thus, without significantly affecting cell growth and proliferation (Figure 1D; Figure S1E), lack of 7SK leads to subtle alterations in genome-wide RNAPII nascent transcription. For the upregulated genes, the pausing index (PI) that gives a measure of RNAPII enrichment in the promoter-proximal region relative to the GB (Figure S2C) was significantly reduced (Figure S2G), suggesting that lack of 7SK may also affect pausing.

Generation of transcriptionally engaged RNAPII metaprofiles over all protein-coding genes or heatmaps over the TSS regions confirms reduced promoter-proximal RNAPII occupancy in 7SK KO cells (Figure 2A; Figures S3A and S3B). In contrast, RNAPII densities in the GB and beyond the TES are comparable in 7SK KO and HAP1 cells (Figure 2A; Figures S3A and S3C). Representative mNET-seq profiles of the *RTF2*, *WDR25*, *AGO4*, *STX7*, and *HELQ* genes illustrate the reduced RNAPII occupancy at the TSS, but not over the GB, in the absence of 7SK (Figure S3D). Chromatin immunoprecipitation followed by quantitative PCR (ChIP-qPCR) confirmed that the lack of 7SK reduces interactions of both RNAPII and the NELF pausing factor NELF-E with the promoter regions of the *HELQ* and *STX7* genes (Figure 2B). Closer inspection of our mNET-seq data revealed that in 7SK KO cells, the TSS regions of long non-coding RNA (lncRNA), PROMPT, and eRNA genes also exhibit reduced RNAPII association (Figure 2C; Figure S3E). Thus, establishment and/or maintenance of efficient promoter-proximal RNAPII pausing on both protein-coding and non-coding genes requires the 7SK snRNP.

Apparently, the most efficiently expressed genes show the strongest promoter-proximal pausing (Figure S2B), and this is

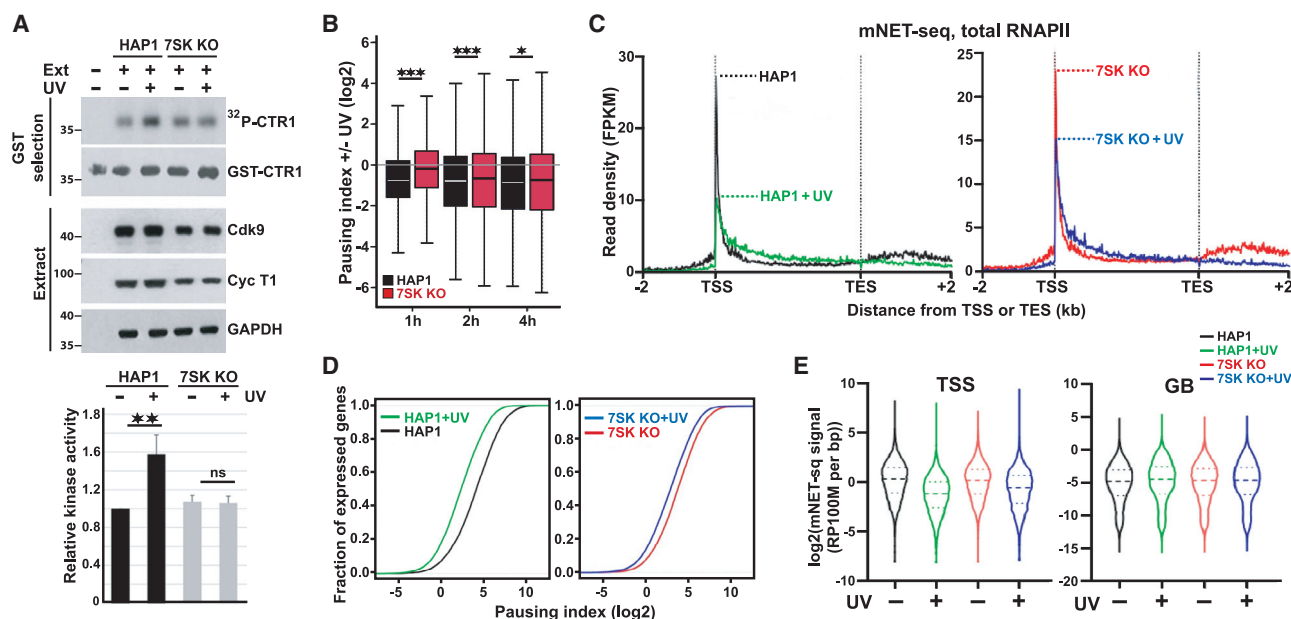


Figure 3. 7SK/P-TEFb promotes RNAPII pause release following UV irradiation

(A) *In vitro* Cdk9 kinase assay. In the presence of γ - 32 P-ATP, recombinant Spt5-CTR1 fused to GST (GST-CTR1) was incubated with extracts prepared from UV-treated or non-treated HAP1 and 7SK KO cells. Cdk9-dependent CTR1 phosphorylation was measured by autoradiography after purification of GST-CTR1 on glutathione resin. The purified GST-CTR1 and endogenous Cdk9, Cyc T1, and GAPDH levels were controlled by western blotting. Phosphorimager quantitation of CTR1 phosphorylation derived from three independent experiments (bottom panel). ** $p < 0.01$, determined by Student's *t* test.

(B) Boxplots comparing the PI ratios (\pm UV) between HAP1 (black) and 7SK KO (red) cells 1, 2, and 4 h after UV irradiation. * $p < 0.05$; *** $p < 0.001$, determined by Wilcoxon test.

(C) Metagenome analysis of RNAPII occupancy measured by mNET-seq on protein-coding genes before and after UV irradiation of HAP1 (left) and 7SK KO cells (right).

(D) Cumulative distribution functions comparing the PI in HAP1 (left) and 7SK KO (right) cells before and after UV exposure.

(E) Violin plots depicting read quantifications at TSS and GB in HAP1 and 7SK KO cells. Thick dotted lines indicate the median, while the thin ones represent the interquartile range (25%–75%). See also Figure S4.

markedly reduced in the absence of 7SK (Figure 2D; Figure S3F). Because HAP1 and 7SK KO cells possess comparable levels of active P-TEFb (Figure 1E) and mNET-seq failed to detect an increase of RNAPII over GBs, it is unlikely that the lack of 7SK causes uncontrolled release of poised RNAPII (Figure 2D; Figure S3F). Thus, we conclude that the 7SK snRNP promotes stable RNAPII pausing across the genome with the strongest impact on highly expressed/paused genes.

7SK/P-TEFb promotes RNAPII pause release following UV irradiation

In response to stress stimuli, active P-TEFb is rapidly released from the 7SK/P-TEFb snRNP (Nguyen et al., 2001). One hour after UV irradiation, an *in vitro* kinase assay detected an approximately 1.6-fold increase of Cdk9 activity in HAP1 cells, while in 7SK KO cells, Cdk9 activity did not increase (Figure 3A). To test the potential contribution of 7SK/P-TEFb to the stress response, we compared nascent RNAPII transcription in UV-irradiated HAP1 and 7SK KO cells by mNET-seq during the early recovery phase (0–4 h). UV treatment is expected to shut down RNAPII transcription at both initiation and elongation stages, presumably to limit production of aberrant transcripts and to facilitate lesion repair (Giono et al., 2016). Indeed, 2 and 4 h after

UV irradiation, we observed a pronounced depletion of actively transcribing RNAPII at both TSS and GB in both HAP1 and 7SK KO cells, indicating that 7SK/P-TEFb is not required for the UV-induced reduction of RNAPII transcription (Figure S4A).

However, 1 h after UV irradiation, when P-TEFb was already released from 7SK/P-TEFb in HAP1 cells, we detected a profound transcriptional impact of the lack of 7SK. Calculation of the PI ratios from two independent mNET-seq experiments followed by RNAPII metaprofile analysis confirmed that UV treatment of HAP1 cells released poised RNAPII from promoter-proximal sites, leading to a consequential increase of elongating RNAPII over the GB (Lavigne et al., 2017; Figures 3B and 3C; Figure S4B). However, UV-induced release of poised RNAPII was substantially reduced in 7SK KO cells (see also Figures S4C–S4E). To further illustrate the UV-provoked transition of RNAPII from pausing to elongation, we calculated PI for individual genes in both HAP1 and 7SK KO cells (Figure 3D). As expected, UV treatment of HAP1 cells provoked a marked decrease in PI (RNAPII depletion at promoters relative to GBs), which was strongly attenuated in 7SK KO cells. Importantly, the PI changes in 7SK KO cells originated from both higher mNET-seq signals at the TSS and reduced signals within the GB (Figure 3E; Figure S4A). Based on these results, we conclude that the

7SK/P-TEFb snRNP is required for quick release of paused RNAPII after UV irradiation, resulting in a transcriptional “wave” that might enhance lesion detection and repair (Lavigne et al., 2017). Because propagation of the UV-triggered transcription wave is compromised in 7SK KO cells, they may suffer from reduced DNA repair efficiency and higher mutational rates.

7SK/P-TEFb is required for UV-induced transcriptional reprogramming

Besides provoking global transcriptional repression, UV irradiation activates a set of key responsive genes to enable a pro-survival transcriptional response (Christmann and Kaina, 2013). mNET-seq analysis of HAP1 cells confirmed transcriptional suppression of more than half of the 14,000 analyzed protein-coding genes 4 h after UV treatment, but it also identified 2,998 genes that were quickly upregulated at least 2-fold within 1 h after UV irradiation (Figure 4A). In 7SK KO cells, however, at least 498 early-responsive genes showed impaired transcriptional activation 1 h after UV exposure, indicating that 7SK is required for proper UV-induced transcriptional reprogramming (Figure 4B). These 7SK-dependent UV-responsive genes encode key factors implicated in apoptosis, cell proliferation, signaling pathways, and cellular response to stimuli (Figure S5A). As an example, the mNET-seq profile of the 7SK-dependent *GADD45B* DNA-damage response gene is shown in Figure 4C. The transcriptional activation defect of the *GADD45B* gene was confirmed by RNAPII ChIP-qPCR analysis in 7SK and 7SKex KO cells (Figure 4D; Figure S5B). Measuring the relative levels of *GADD45B*, *SGK1*, and *RND1* mRNAs and pre-mRNAs by qRT-PCR confirmed their reduced inductions in 7SK, 7SKex, and *Larp7* KO cells (Figure 4E; Figures S5C and S5D). Compared with HAP1 cells, the 7SK RST cells, which accumulate 7SK with 60%–70% efficiency (Figure 1A), showed only partial *GADD45B*, *SGK1*, and *RND1* activations (Figures S5B and S5E). Analysis of the mNET-seq metaprofiles of the 498 7SK-dependent UV-responsive genes revealed that their transcriptional defects arise, at least partially, from default RNAPII pause release (Figure 4F; Figure S5F). This suggests that besides supporting DNA lesion scanning, UV-induced release of paused RNAPII is also critical for controlling expression of early-responsive genes. The transcriptional wave emanating from UV-triggered RNAPII pause release has a reduced elongation speed (400 bp/min instead of 2 kb/min); therefore, it favors transcription of shorter genes (Williamson et al., 2017). Consistent with this, genes readily induced in response to UV tend to be shorter (Figure 4G). The short average length of early-responsive genes may allow their productive transcription by slowly elongating RNAPII and mitigate the probability of RNAPII encountering bulky photo-products interfering with its progression (McKay et al., 2004).

Defective DNA lesion scanning and reduced expression of key early-response genes may have deleterious effects on DNA damage response efficiency and cell fate (McKay et al., 2004). Accordingly, we compared the recovering abilities of HAP1 cells expressing or lacking 7SK snRNA after irradiation with a moderate dose of UV (10 J/m²). The 7SK KO cells failed to reestablish efficient cell proliferation 3 days after UV treatment, whereas HAP1 and 7SK RST cells efficiently recovered from UV-induced stress (Figure 4H). Clonogenic assays confirmed that cell sur-

vival was significantly reduced in the absence of 7SK or *Larp7* (Figure 4I; Figure S5G), which may reflect increased apoptosis during the first days following UV exposure. Thus, we conclude that the lack of 7SK snRNA provokes cellular hypersensitivity to UV.

7SK/P-TEFb stimulates UV-dependent recruitment of key elongation factors

Next, we measured the occupancy of the NELF and DSIF pausing factors on selected 7SK-dependent early-responsive genes by ChIP-qPCR in HAP1 and 7SK KO cells. Under normal growth conditions, we detected significantly lower NELF-E levels at the TSS of the *GADD45B*, *RND1*, and *SGK1* genes in 7SK KO cells, mirroring reduced RNAPII pausing in the absence of 7SK (Figure 5A; Figure S6A). More importantly, UV irradiation resulted in efficient promoter-proximal NELF-E clearing in both cell lines, demonstrating that NELF dissociation occurs in the absence of 7SK/P-TEFb. The Spt5 subunit of DSIF and RNAPII showed highly similar distribution profiles along the *GADD45B* transcription unit (Figure 5B; Figure S6B). In UV-irradiated HAP1 cells, the level of DSIF and RNAPII decreased at the TSS and increased in the GB, reflecting RNAPII pause release and gene activation. In 7SK KO cells, this UV-induced increase in the GB was largely attenuated for both RNAPII and DSIF. Accordingly, the Spt5/RNAPII ratio was highly comparable in HAP1 and 7SK KO cells before and after UV treatment alongside the entire gene, showing that association of DSIF with RNAPII is not affected by the lack of 7SK (Figure S6C).

To monitor P-TEFb occupancy on the *GADD45B* and *SGK1* TSS in the presence and absence of 7SK/P-TEFb, we performed ChIP-qPCR analysis with an anti-Cdk9 antibody in HAP1 and 7SK KO cells (Figure 5C; Figure S6D). As expected, we detected largely increased Cdk9 association with the TSS regions of *GADD45B* and *SGK1* upon UV irradiation of HAP1 cells. In contrast, UV treatment failed to augment Cdk9 association with the TSS regions of *GADD45B* and *SGK1* in 7SK KO cells, demonstrating that 7SK/P-TEFb is required for UV-induced P-TEFb recruitment. Because P-TEFb is frequently delivered to active genes as a component of SECs (Luo et al., 2012), we performed ChIP with an antibody against the AFF4 subunit of SECs. After UV irradiation, the association of AFF4 with the TSS of the *GADD45B* and *RND1* genes increased in HAP1, but not in 7SK KO cells (Figure 5D; Figure S6E), demonstrating that 7SK is required for UV-induced loading of SECs onto these stress-response genes. Thus, we conclude that compromised P-TEFb recruitment, mainly or exclusively in the form of SECs, may be responsible for the weak induction of early-response genes in 7SK KO cells.

We also followed recruitment of two other key RNAPII elongation factors, the PAF1 complex (PAF1C) and SPT6. Although SPT6 is required for both the release and subsequent elongation of RNAPII (Vos et al., 2018), the role of PAF1C, composed of Paf1, Cdc73, Ctr9, Leo1, and Ski8, is still controversial because it has been reported to function both in enforcement and in releasing of RNAPII pausing (Vos et al., 2018; Yu et al., 2015). Upon UV irradiation, both SPT6 and Paf1 showed dramatically increased *GADD45B* and *SGK1* TSS occupancies in HAP1 cells, while in 7SK KO cells they showed significantly weaker

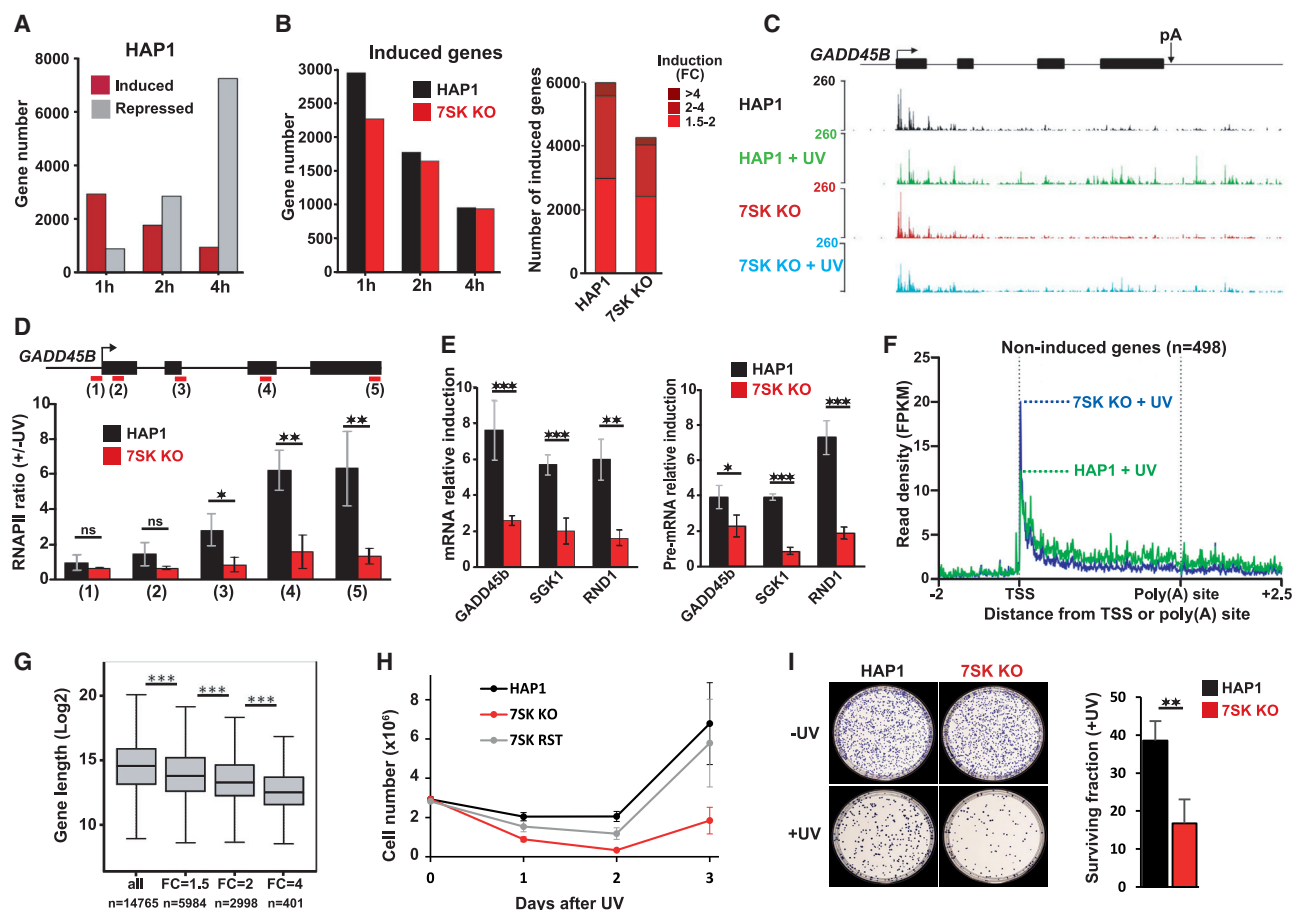


Figure 4. 7SK/P-TEFb is required for UV-induced transcriptional reprogramming

(A) Bar charts indicate the numbers of HAP1 genes either induced or repressed at least 2-fold 1, 2, and 4 h after UV exposure, as assessed by mNET-seq.

(B) Comparison of UV-induced gene expressions in HAP1 and 7SK KO cells. Left panel compares the numbers of UV-induced (at least 2-fold) genes in HAP1 and 7SK KO cells 1, 2, and 4 h after UV treatment. Right panel compares the numbers and activation levels of UV-induced (at least 1.5-fold, see color code) genes in HAP1 and 7SK KO cells 1 h after UV irradiation.

(C) RNAPII occupancy on the human *GADD45B* gene determined by mNET-seq analyses of UV-treated or non-treated HAP1 and 7SK KO cells. Schematic structure of the *GADD45B* gene with the corresponding mNET-seq positive strand reads are shown.

(D) Quantitative ChIP analyses of endogenous RNAPII occupancy on the *GADD45B* gene in HAP1 and 7SK KO cells. Signals are represented as fold-change enrichments induced by UV treatment. Positions of the PCR-amplified fragments (1–5) are indicated. * $p < 0.05$; ** $p < 0.01$, determined by Student's *t* test.

(E) qRT-PCR quantification of the indicated UV-induced mRNAs (left) and pre-mRNAs (right). The results were normalized to non-irradiated controls, and the error bars represent standard deviations from at least three independent experiments. * $p < 0.05$; ** $p < 0.01$; *** $p < 0.001$, determined by Student's *t* test.

(F) Metagene analysis of RNAPII occupancy on 498 genes, which are not properly induced by UV irradiation in the absence of 7SK.

(G) Boxplots illustrating that genes strongly induced by UV tend to be shorter. The fold-change induction (FC) and the numbers of analyzed genes are indicated. *** $p < 0.001$, determined by Wilcoxon test.

(H) Growth curves of HAP1, 7SK KO, and 7SK RST cells after irradiation with low dose of UV (10 J/m^2). Error bars represent standard deviations from three independent experiments.

(I) Clonogenic assays performed on HAP1 and 7SK KO cells treated with moderate dose of UV (10 J/m^2). The surviving fraction was determined by counting the number of colonies formed by the surviving cells relative to the non-irradiated control cells. ** $p < 0.01$, determined by Student's *t* test.

pA, polyA site. See also Figure S5.

recruitments (Figure 5E; Figure S6F). The decreased PAF1C and SPT6 recruitment was not a consequence of reduced RNAPII pausing, because the level of paused RNAPII on *GADD45B* was comparable in UV-treated HAP1 and 7SK KO cells (Figure 5B). Therefore, we conclude that efficient PAF1C and SPT6 recruitment to the *GADD45B* and *SGK1* early-response genes requires 7SK/P-TEFb. Importantly, the 7SK-dependent recruit-

ment of AFF4, PAF1, and SPT6 is specific to UV-induced genes, as it was not observed on the *HELQ* non-responsive gene (Figure S6G). Because P-TEFb, SECs, PAF1C, and SPT6 positively regulate RNAPII elongation beyond pause release (Hou et al., 2019), their compromised recruitment to early-responsive genes in 7SK KO cells could lead to reduced elongation rates and reduced synthesis of full-length transcripts.

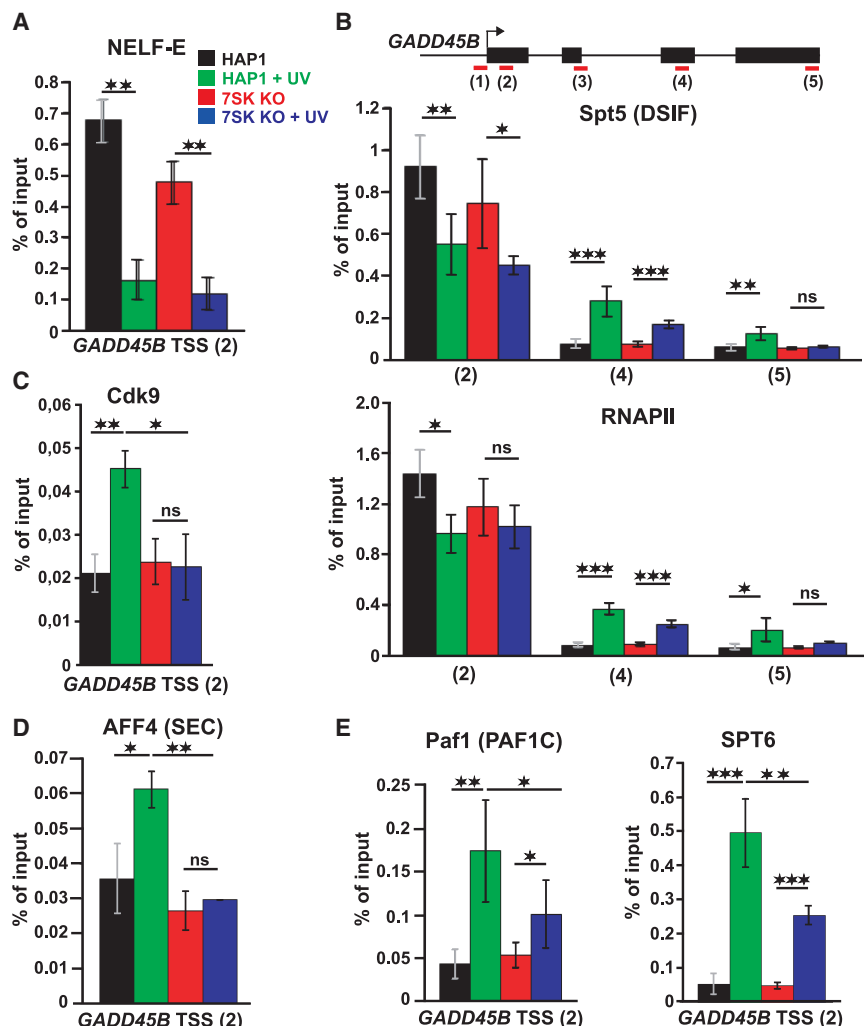


Figure 5. 7SK/P-TEFb stimulates UV-dependent recruitment of key elongation factors

(A) Quantitative ChIP analyses of NELF-E occupancy at the TSS of *GADD45B* in HAP1 and 7SK KO cells before and 1 h after UV exposure. For position of the PCR-amplified fragment (2), see (B). Signals are represented as % of input. For all panels, * $p < 0.05$; ** $p < 0.01$; *** $p < 0.001$, determined by Student's t test. Error bars represent standard deviations from at least three independent experiments.

(B) Quantitative ChIP analysis of RNAPII and Spt5 occupancy on the *GADD45B* gene in HAP1 and 7SK KO cells before and 1 h after UV exposure. Positions of the PCR-amplified fragments are indicated below the schematic diagram of *GADD45B*.

(C) Quantitative ChIP analyses of AFF4 occupancy at the TSS of *GADD45B* in HAP1 and 7SK KO cells before and 1 h after UV exposure.

(D) Quantitative ChIP analyses of AFF4 (SEC) occupancy at the TSS of *GADD45B* in HAP1 and 7SK KO cells before and 1 h after UV exposure.

(E) Quantitative ChIP analyses of PAF1 and SPT6 occupancies at the TSS of *GADD45B* in HAP1 and 7SK KO cells before and 1 h after UV irradiation. See also Figure S6.

Together, our results suggest that the 7SK/P-TEFb snRNP stimulates expression of stress-responsive genes through directly providing active P-TEFb for the RNAPII transcription machinery to promote efficient pause release and subsequent recruitment of key elongation factors.

P-TEFb is extracted from nucleoplasmic 7SK/P-TEFb during the UV response

Defective activation of some early-responsive genes in 7SK KO cells seems to arise mainly from insufficient P-TEFb/SECs recruitment (Figures 5C and 5D; Figures S6D and S6E). It has been proposed that inactive 7SK/P-TEFb can be loaded onto selected gene promoters for onsite P-TEFb extraction to support synchronous gene activation in response to environmental cues, including UV irradiation (Gudipaty et al., 2015; McNamara et al., 2013). However, ChIP-qPCR failed to detect MePCE association with the promoter regions of human *GADD45B* and other genes, including *HNRNPH1*, on which 7SK/P-TEFb loading had been reported in mouse (Ji et al., 2013; Figure 6A; Figure S7A). In contrast, the previously reported association of MePCE with

the 7SK snRNA gene was readily reproduced (Xue et al., 2010) (Figure 6A). MePCE association with the 7SK gene is transcription dependent, because it is largely reduced by UV irradiation and fully abolished by disruption of 7SK expression (Figure 6A; Figure S7B).

Because ChIP failed to confirm 7SK/P-TEFb association with protein-coding genes (see also Egloff et al., 2017), we performed chromatin isolation by RNA purification followed by sequencing

(ChIRP-seq) experiments to determine the genome-wide chromatin association of 7SK snRNP. After crosslinking and DNA shearing, affinity selection with biotinylated oligonucleotides recovered about 75% of the total 7SK snRNA from both control and UV-irradiated cells (Figure S7C). Deep sequencing of the co-purified DNA fragments failed to detect significant 7SK association with protein-coding genes in non-treated or UV-treated HAP1 cells, because the non-specific ChIRP-seq signals were even higher in 7SK KO control cells (Figure 6B; Figure S7D). Likewise, the 498 7SK-dependent early-response genes showed no specific association with 7SK snRNA in HAP1 cells (Figure 6C; Figure S7E). However, the previously detected association of 7SK snRNP with RNAPII-transcribed snRNA genes and some protein-coding genes, for instance, *EEF1A1* (Egloff et al., 2017; Flynn et al., 2016; Mumbach et al., 2019), was confirmed by our analysis (Figure S7F). Thus, ChIRP-seq data strongly argue against the prevalent association of the 7SK snRNP with human genes, with the exception of a few transcription units.

We next measured the relative association levels of P-TEFb and HEXIM1 with chromatin isolated from HAP1 and 7SK KO

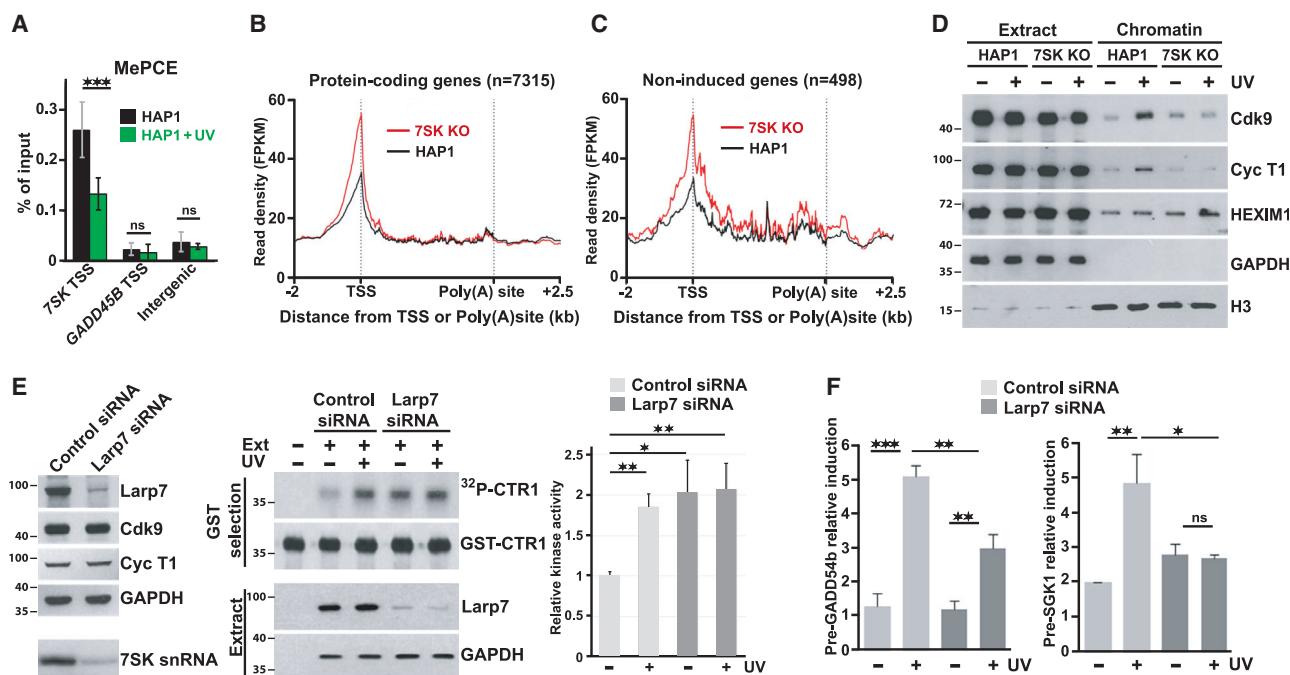


Figure 6. P-TEFb is extracted from nucleoplasmic 7SK/P-TEFb during the UV response

(A) Quantitative ChIP analyses of MePCE occupancy at the TSS of *7SK* and *GADD45B* genes in HAP1 cells before and 1 h after UV exposure. Signals are represented as % of input. * $p < 0.05$; ** $p < 0.01$; *** $p < 0.001$, determined by Student's *t* test.

(B) Metagene analysis of 7SK RNA occupancy on protein-coding genes in HAP1 cells, as measured by genome-wide ChIRP-seq analysis. Signals detected in 7SK KO cells are considered as non-specific.

(C) Metagene analysis of 7SK RNA occupancy on the 498 improperly induced genes after UV exposure of 7SK KO cells.

(D) UV-induced 7SK-dependent chromatin association of P-TEFb. Chromatin was isolated from HAP1 and 7SK KO cells either treated or non-treated with UV light (40 J/m²). Cdk9, Cyc T1, HEXIM1, GAPDH, and histone H3 levels in the total extracts and chromatin fractions were measured by western blotting.

(E) *In vitro* Cdk9 kinase assay. In the presence of γ -³²P-ATP, GST-fused recombinant Spt5-CTR1 (GST-CTR1) was incubated with total extracts prepared from UV-treated or non-treated HAP1 cells that had been transfected with Larp7-specific or control siRNAs. CTR1 phosphorylation by Cdk9 was measured by autoradiography after purification of GST-CTR1. The levels of purified GST-CTR1, endogenous Larp7, and GAPDH were analyzed by western blotting. Radioactive signals obtained from at least three independent experiments were quantitated by phosphorimager. Depletion of 7SK snRNP by a Larp7-specific siRNA was controlled by northern (7SK snRNA) and western (Larp7, Cdk9, Cyc T1, and GAPDH) blot analysis. * $p < 0.05$; ** $p < 0.01$, determined by Student's *t* test.

(F) qRT-PCR analysis of *GADD45B* and *SGK1* pre-mRNAs in control- and Larp7-depleted HAP1 cells before and 1 h after UV irradiation. Signals were normalized to B-ACTIN mRNA levels. Bars indicate average values of three independent experiments with error bars representing standard deviations. * $p < 0.05$; ** $p < 0.01$; *** $p < 0.001$, determined by Student's *t* test.

FPKM, fragments per kilobase per million mapped reads. See also Figure S7.

cells before and after UV irradiation (Figure 6D). One hour after UV exposure, both Cdk9 and Cyc T1 showed increased chromatin association in HAP1, but not in 7SK KO cells. This indicates that UV-induced recruitment of nucleoplasmic P-TEFb to chromatin depends on the 7SK snRNP. However, in contrast with P-TEFb, HEXIM1 showed no increased chromatin association in UV-treated HAP1 cells, arguing against 7SK/HEXIM1-mediated P-TEFb loading onto the chromatin. We propose that upon UV irradiation, active P-TEFb is directly extracted from the nucleoplasmic 7SK/P-TEFb snRNP and used for gene activation.

To confirm this hypothesis, we depleted the majority of 7SK snRNP from HAP1 cells by small interfering RNA (siRNA)-mediated disruption of Larp7 expression (Figure 6E). As reported earlier (Ji et al., 2014), transient diminution of 7SK snRNP accumulation strongly increased the level of active P-TEFb, even exceeding the P-TEFb level measured in UV-irradiated HAP1 control cells. However, contrary to their high P-TEFb levels, the

7SK-depleted HAP1 cells failed to sustain full activation of the *GADD45B* and *SGK1* genes upon UV irradiation (Figure 6F), demonstrating that free P-TEFb is unable to support activation of 7SK-dependent stress-response genes, and that the presence of 7SK/P-TEFb is critical for efficient RNAPII transcriptional reprogramming during the UV response.

DISCUSSION

Conversion of promoter-proximally paused RNAPII into elongating polymerase depends on the Cdk9 activity of P-TEFb, which is controlled by the 7SK snRNP through sequestering active P-TEFb into inactive 7SK/P-TEFb. The 7SK/P-TEFb snRNP functions as a dynamic P-TEFb reservoir from which active P-TEFb can be mobilized either in the nucleosol or on the promoter-proximal chromatin next to the paused RNAPII (D'Orso and Frankel, 2010; McNamara et al., 2013, 2016; Nguyen et al., 2001; Yang et al., 2001). Cellular stresses trigger

rapid P-TEFb release from the 7SK/P-TEFb snRNP to activate Cdk9, but paradoxically, stress conditions often halt transcription. Therefore, the biological significance of the 7SK/P-TEFb complex remained difficult to ascertain. Here, we have generated a human 7SK KO cell line that accumulates only the active form of P-TEFb and lacks its inactive 7SK-associated form (Figure 1). Because the Cdk9 activities in HAP1 and 7SK KO cells are highly comparable, the 7SK KO cells provide an excellent tool to assess the impact of the lack of inactive 7SK/P-TEFb on RNAPII transcription under normal and stress conditions.

Although the 7SK/P-TEFb snRNP has been implicated in controlling the global P-TEFb activity and also in P-TEFb loading onto promoter-proximal chromatin, under normal culture conditions, the 7SK KO cells showed no significant growth and proliferation deficiencies, and they displayed only modest alterations in genome-wide transcription dynamics. This demonstrates that free P-TEFb can support basal transcription and also suggests that the 7SK/P-TEFb snRNP might only fine-tune gene expression, at least in cultured cells.

7SK depletion reduced transcriptionally engaged RNAPII at the pause sites of most genes, with the strongest effects on highly expressed paused genes. The mechanism reducing genome-wide RNAPII pausing in the absence of 7SK/P-TEFb remains unclear. In theory, RNAPII pausing could be reduced by decreased initiation or by perturbed pause establishment and/or release. Supporting the second possibility, 7SK KO cells showed reduced TSS occupancy by the NELF pausing factor, the association of which is directly regulated by P-TEFb activity (Core and Adelman, 2019; Figure 5A; Figure S6A). Because reduced mNET-seq reads at pause sites are not accompanied by increased reads in GBs in 7SK KO cells, we can exclude the possibility that the reduced RNAPII pausing is a consequence of increased pause release (Figure 2D). Interestingly, previous ChIP-seq (Ji et al., 2013; McNamara et al., 2016) and 7SK ChIRP-seq (Flynn et al., 2016) reported on low levels of 7SK snRNP associated with most protein-coding gene promoters, raising the possibility that 7SK or the 7SK/P-TEFb snRNP might directly participate in RNAPII pause control. However, our attempts to localize 7SK snRNP components on protein-coding genes failed (Figure 6; Egloff et al., 2017). 7SK ChIRP-seq analyses confirmed that 7SK snRNP loading is restricted to RNAPII-transcribed spliceosomal snRNA and a few protein-coding genes (Figure S7F; Egloff et al., 2017; Flynn et al., 2016; Mumbach et al., 2019). It is important to note that ChIRP-seq conducted on HAP1, but also on 7SK KO cells, engendered high background signals at TSSs (Figures 6B and 6C), indicating that high non-specific signals on actively transcribed genes can skew results. Therefore, including KO cell lines as negative controls seems to be critical for these experiments. In conclusion, although our results indicate that the 7SK/P-TEFb snRNP contributes to the maintenance of an efficient RNAPII pause at promoter-proximal sites, they argue against prevalent 7SK/P-TEFb association with protein-coding genes.

mNET-seq analyses of UV-irradiated HAP1 and 7SK KO cells during the early recovery phase highlighted several anomalies of UV-induced transcriptional reprogramming in 7SK KO cells.

Within the first hour after UV treatment of HAP1 cells, paused RNAPII is released from promoter-proximal sites, and this is followed by a progressive transcriptional shutdown during the next 3 h (Figures 3 and 4A). This timing allows transcription of early stress-response genes before genome-wide transcriptional repression is fully established. Because 7SK/P-TEFb disassembly occurs within the first hour after UV irradiation, it is expected to influence the early events of the UV-induced transcriptional response. Indeed, we found that the 7SK/P-TEFb snRNP is required for rapid and synchronous UV-triggered promoter-proximal clearance of paused RNAPII to generate an elongation wave that is believed to sense DNA damages on all transcribed genes (Lavigne et al., 2017; see model in Figure 7). When it encounters DNA lesions, stalled RNAPII could initiate repair by the TC-NER system (Lindsey-Boltz and Sancar, 2007). The stress-induced P-TEFb-dependent RNAPII transcription wave is restricted to about 25 kb downstream of the TSS (Williamson et al., 2017). This primarily allows expression of short genes, such as early-response genes, the activation of which is critical for efficient DNA damage response (Christmann and Kaina, 2013; McKay et al., 2004; Tufegdžić Vidaković et al., 2020; Figure 4G). The UV-induced elongation boost is largely attenuated in 7SK KO cells, where 7SK/P-TEFb disassembly cannot provide extra P-TEFb to trigger the increased transition of RNAPII into productive elongation (Figure 3A). In 7SK KO cells, a fraction of early-response genes show impaired transcriptional activation arising from compromised RNAPII pause release (Figure 4F). In line with this conclusion, loading of P-TEFb/SEC, as well as other key elongation factors, such as PAF1C and SPT6, onto the promoter-proximal regions of 7SK-dependent early-response genes is compromised in the absence of 7SK/P-TEFb (Figure 5; Figure S6). On these genes, effective dissociation of NELF after UV exposure is not sufficient to release RNAPII from pause sites in 7SK KO cells, suggesting that other factors govern stress-induced pause release, as recently suggested by rapid NELF depletion strategies (Aoi et al., 2020). P-TEFb has been demonstrated to facilitate PAF1C binding that, in turn, could help RNAPII release from pausing (Vos et al., 2018; Yu et al., 2015) and positively regulate downstream RNAPII elongation and progression (Hou et al., 2019). In addition, P-TEFb-dependent CTD linker phosphorylation promotes SPT6 binding to the RNAPII elongation complex (Vos et al., 2018), which also stimulates transcription elongation *in vivo* (Ardehali et al., 2009; Nojima et al., 2018). Finally, SECs are active elongation factor complexes that are required for rapid transcriptional gene induction (Luo et al., 2012). Thus, defective recruitment of these factors following UV irradiation could have synergic effects on RNAPII pause release and elongation. Because the elongation rate governs co-transcriptional alternative splicing (Muñoz et al., 2009) and expression of alternative isoforms (Williamson et al., 2017), the impact of 7SK loss on transcription could even be reinforced by RNA-processing defects.

Nuclear fractionation experiments showed that upon UV-induced disassembly of the nucleosolic 7SK/P-TEFb snRNP, the released P-TEFb is recruited to chromatin (Figure 6D). Importantly, increasing the nuclear P-TEFb activity of HAP1 cells through transient disruption of the 7SK/P-TEFb snRNP

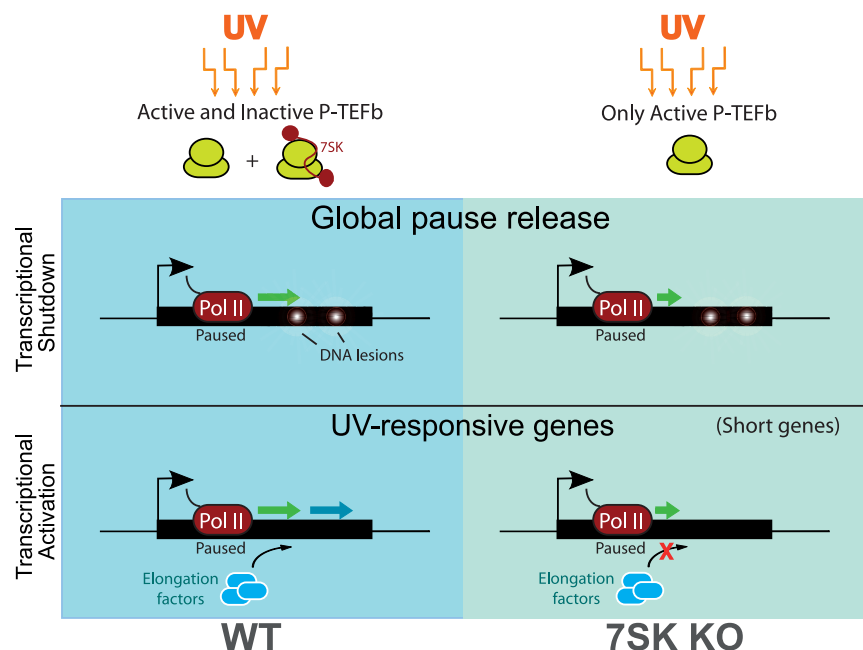


Figure 7. The 7SK/P-TEFb snRNP controls UV-induced transcriptional reprogramming

Schematic illustration of UV-induced gene expression programs in cultured human HAP1 cells either expressing (wild type [WT]) or lacking (7SK KO) 7SK/P-TEFb. Upon UV irradiation, paused RNAPII is efficiently (WT) or weakly (7SK KO) released into GBs (as indicated by green arrows) to scan DNA for lesions (white dots) before progressive transcriptional shutdown takes place. In the meantime, in WT, but not in 7SK KO cells, a set of key UV-responsive genes undergoes selective transcriptional activation (blue arrow), supported by efficient RNAPII pause release and productive elongation. The transcriptional defects in 7SK KO cells are likely caused by their inability to transiently augment P-TEFb activity, compromising efficient RNAPII pause release and proper recruitment of key elongation factors.

by RNA interference failed to properly activate early-response genes upon UV irradiation, demonstrating that free P-TEFb cannot support efficient gene activation (Figures 6E and 6F). We propose that specific transcription factors extract active P-TEFb from the nucleosolic 7SK/P-TEFb and after incorporation into SECs, they target it to the promoter-proximal regions of selected genes. The exact mechanism may depend on the stress stimulus. The bromodomain protein 4 (BRD4) and the RNA-binding motif protein 7 (RBM7) have been reported to release P-TEFb from the 7SK/P-TEFb snRNP under stress conditions (Bugai et al., 2019; Yang et al., 2005), and therefore are possible candidates for triggering UV-induced recruitment of P-TEFb to chromatin.

In summary, our data implicate relocation of P-TEFb from the nucleoplasmic 7SK/P-TEFb snRNP to the chromatin as a major regulatory step of UV-induced stress response, which is necessary to release genome-wide RNAPII pausing and to induce transcription of key responsive genes (Figure 7). Therefore, the 7SK/P-TEFb snRNP likely exerts genome-protective effects through promoting efficient DNA damage response that could be critical for cell fate, as suggested by the increased sensitivity to radiations of 7SK KO cells in the first few days after UV exposure (Figures 4H and 4I).

STAR★METHODS

Detailed methods are provided in the online version of this paper and include the following:

- KEY RESOURCES TABLE
- RESOURCE AVAILABILITY
 - Lead contact
 - Materials availability

- Data and code availability
- EXPERIMENTAL MODEL AND SUBJECT DETAILS
- METHOD DETAILS
 - General procedures
 - UV irradiation
 - Cell proliferation assays
 - Clonogenic assays
 - EU incorporation assays
 - Inactivation of 7SK and LARP7 genes by CRISPR/Cas9
 - Glycerol gradient analysis
 - siRNA-mediated Larp7 knockdown
 - Chromatin fractionation
 - Immunoprecipitation and protein analysis
 - Chromatin immunoprecipitation
 - Mammalian native elongating transcript sequencing (mNET-seq)
 - Chromatin isolation by RNA purification (ChIRP) and deep sequencing
 - mNET-seq data processing
 - ChIRP-seq data processing
 - RNA-seq data processing
 - Transcription unit (TU) definition
 - Reads quantification
 - Metagene profiles
 - Fluorescence *in situ* hybridization
 - RNA analysis
 - *In vitro* kinase assay
- QUANTIFICATION AND STATISTICAL ANALYSIS

SUPPLEMENTAL INFORMATION

Supplemental information can be found online at <https://doi.org/10.1016/j.celrep.2021.108965>.

ACKNOWLEDGMENTS

We are indebted to Dr. R.P. Fischer (Icahn School of Medicine at Mount Sinai, New York, NY, USA) for providing us with the GST-CTR1 construct. Our work was supported by grants from INSERM Plan Cancer, ANRS (France Recherche Nord & Sud Sida-HIV Hépatites), and Agence Nationale de la Recherche (ANR-18-CE12-0008 to T.K.).

AUTHOR CONTRIBUTIONS

C.S. and S.E. carried out experiments. S.E., S.M., and T.K. conceived and designed experiments. C.S., M.T. and P.G.P.M. analyzed the mNET-seq and ChIRP-seq data. S.E. and T.K. wrote the manuscript.

DECLARATION OF INTERESTS

The authors declare no competing interests.

Received: August 31, 2020

Revised: January 27, 2021

Accepted: March 17, 2021

Published: April 13, 2021

REFERENCES

- Adelman, K., and Lis, J.T. (2012). Promoter-proximal pausing of RNA polymerase II: emerging roles in metazoans. *Nat. Rev. Genet.* **13**, 720–731.
- Aoi, Y., Smith, E.R., Shah, A.P., Rendleman, E.J., Marshall, S.A., Woodfin, A.R., Chen, F.X., Shiekhattar, R., and Shilatifard, A. (2020). NELF Regulates a Promoter-Proximal Step Distinct from RNA Pol II Pause-Release. *Mol. Cell* **78**, 261–274.e5.
- Ardehali, M.B., Yao, J., Adelman, K., Fuda, N.J., Petesch, S.J., Webb, W.W., and Lis, J.T. (2009). Spt6 enhances the elongation rate of RNA polymerase II in vivo. *EMBO J.* **28**, 1067–1077.
- Barrandon, C., Bonnet, F., Nguyen, V.T., Labas, V., and Bensaude, O. (2007). The transcription-dependent dissociation of P-TEFb-HEXIM1-7SK RNA relies upon formation of hnRNP-7SK RNA complexes. *Mol. Cell. Biol.* **27**, 6996–7006.
- Bugai, A., Quresma, A.J.C., Friedel, C.C., Lenasi, T., Duster, R., Sibley, C.R., Fujinaga, K., Kukanja, P., Hennig, T., Blasius, M., et al. (2019). P-TEFb Activation by RBM7 Shapes a Pro-survival Transcriptional Response to Genotoxic Stress. *Mol. Cell* **74**, 254–267.e10.
- Calo, E., Flynn, R.A., Martin, L., Spitale, R.C., Chang, H.Y., and Wysocka, J. (2015). RNA helicase DDX21 coordinates transcription and ribosomal RNA processing. *Nature* **518**, 249–253.
- Castelo-Branco, G., Amaral, P.P., Engström, P.G., Robson, S.C., Marques, S.C., Bertone, P., and Kouzarides, T. (2013). The non-coding snRNA 7SK controls transcriptional termination, poising, and bidirectionality in embryonic stem cells. *Genome Biol.* **14**, R98.
- Chen, Y., Pai, A.A., Herudek, J., Lubas, M., Meola, N., Järvelin, A.I., Andersson, R., Pelechano, V., Steinmetz, L.M., Jensen, T.H., and Sandelin, A. (2016). Principles for RNA metabolism and alternative transcription initiation within closely spaced promoters. *Nat. Genet.* **48**, 984–994.
- Christmann, M., and Kaina, B. (2013). Transcriptional regulation of human DNA repair genes following genotoxic stress: trigger mechanisms, inducible responses and genotoxic adaptation. *Nucleic Acids Res.* **41**, 8403–8420.
- Chu, C., Quinn, J., and Chang, H.Y. (2012). Chromatin isolation by RNA purification (ChIRP). *J. Vis. Exp.* **2012**, 3912.
- Core, L., and Adelman, K. (2019). Promoter-proximal pausing of RNA polymerase II: a nexus of gene regulation. *Genes Dev.* **33**, 960–982.
- D'Orso, I., and Frankel, A.D. (2010). RNA-mediated displacement of an inhibitory snRNP complex activates transcription elongation. *Nat. Struct. Mol. Biol.* **17**, 815–821.
- Darzacq, X., Jádý, B.E., Verheggen, C., Kiss, A.M., Bertrand, E., and Kiss, T. (2002). Cajal body-specific small nuclear RNAs: a novel class of 2'-O-methylation and pseudouridylation guide RNAs. *EMBO J.* **21**, 2746–2756.
- Diribarne, G., and Bensaude, O. (2009). 7SK RNA, a non-coding RNA regulating P-TEFb, a general transcription factor. *RNA Biol.* **6**, 122–128.
- Dobin, A., Davis, C.A., Schlesinger, F., Drenkow, J., Zaleski, C., Jha, S., Batut, P., Chaisson, M., and Gingeras, T.R. (2013). STAR: ultrafast universal RNA-seq aligner. *Bioinformatics* **29**, 15–21.
- Egloff, S., Vitali, P., Tellier, M., Raffel, R., Murphy, S., and Kiss, T. (2017). The 7SK snRNP associates with the little elongation complex to promote snRNA gene expression. *EMBO J.* **36**, 934–948.
- Flynn, R.A., Do, B.T., Rubin, A.J., Calo, E., Lee, B., Kuchelmeister, H., Rale, M., Chu, C., Kool, E.T., Wysocka, J., et al. (2016). 7SK-BAF axis controls pervasive transcription at enhancers. *Nat. Struct. Mol. Biol.* **23**, 231–238.
- Giono, L.E., Nieto Moreno, N., Cambindo Botto, A.E., Dujardin, G., Muñoz, M.J., and Kornblihtt, A.R. (2016). The RNA Response to DNA Damage. *J. Mol. Biol.* **428**, 2636–2651.
- Gressel, S., Schwalb, B., Decker, T.M., Qin, W., Leonhardt, H., Eick, D., and Cramer, P. (2017). CDK9-dependent RNA polymerase II pausing controls transcription initiation. *eLife* **6**, e29736.
- Gudipaty, S.A., McNamara, R.P., Morton, E.L., and D'Orso, I. (2015). PPM1G Binds 7SK RNA and Hexim1 To Block P-TEFb Assembly into the 7SK snRNP and Sustain Transcription Elongation. *Mol. Cell. Biol.* **35**, 3810–3828.
- He, N., Jahchan, N.S., Hong, E., Li, Q., Bayfield, M.A., Marais, R.J., Luo, K., and Zhou, Q. (2008). A La-related protein modulates 7SK snRNP integrity to suppress P-TEFb-dependent transcriptional elongation and tumorigenesis. *Mol. Cell* **29**, 588–599.
- He, N., Liu, M., Hsu, J., Xue, Y., Chou, S., Burlingame, A., Krogan, N.J., Alber, T., and Zhou, Q. (2010). HIV-1 Tat and host AFF4 recruit two transcription elongation factors into a bifunctional complex for coordinated activation of HIV-1 transcription. *Mol. Cell* **38**, 428–438.
- Hou, L., Wang, Y., Liu, Y., Zhang, N., Shamovsky, I., Nudler, E., Tian, B., and Dynlacht, B.D. (2019). Paf1C regulates RNA polymerase II progression by modulating elongation rate. *Proc. Natl. Acad. Sci. USA* **116**, 14583–14592.
- Jang, M.K., Mochizuki, K., Zhou, M., Jeong, H.S., Brady, J.N., and Ozato, K. (2005). The bromodomain protein Brd4 is a positive regulatory component of P-TEFb and stimulates RNA polymerase II-dependent transcription. *Mol. Cell* **19**, 523–534.
- Jeronimo, C., Forget, D., Bouchard, A., Li, Q., Chua, G., Poitras, C., Thérien, C., Bergeron, D., Bourassa, S., Greenblatt, J., et al. (2007). Systematic analysis of the protein interaction network for the human transcription machinery reveals the identity of the 7SK capping enzyme. *Mol. Cell* **27**, 262–274.
- Ji, X., Zhou, Y., Pandit, S., Huang, J., Li, H., Lin, C.Y., Xiao, R., Burge, C.B., and Fu, X.D. (2013). SR proteins collaborate with 7SK and promoter-associated nascent RNA to release paused polymerase. *Cell* **153**, 855–868.
- Ji, X., Lu, H., Zhou, Q., and Luo, K. (2014). LARP7 suppresses P-TEFb activity to inhibit breast cancer progression and metastasis. *eLife* **3**, e02907.
- Jonkers, I., and Lis, J.T. (2015). Getting up to speed with transcription elongation by RNA polymerase II. *Nat. Rev. Mol. Cell Biol.* **16**, 167–177.
- Jonkers, I., Kwak, H., and Lis, J.T. (2014). Genome-wide dynamics of Pol II elongation and its interplay with promoter proximal pausing, chromatin, and exons. *eLife* **3**, e02407.
- Kobbi, L., Demey-Thomas, E., Braye, F., Proux, F., Kolesnikova, O., Vinh, J., Poterszman, A., and Bensaude, O. (2016). An evolutionary conserved Hexim1 peptide binds to the Cdk9 catalytic site to inhibit P-TEFb. *Proc. Natl. Acad. Sci. USA* **113**, 12721–12726.
- Krueger, B.J., Jeronimo, C., Roy, B.B., Bouchard, A., Barrandon, C., Byers, S.A., Searcey, C.E., Cooper, J.J., Bensaude, O., Cohen, E.A., et al. (2008). LARP7 is a stable component of the 7SK snRNP while P-TEFb, HEXIM1 and hnRNP A1 are reversibly associated. *Nucleic Acids Res.* **36**, 2219–2229.
- Larochelle, S., Batliner, J., Gamble, M.J., Barboza, N.M., Kraybill, B.C., Blethrow, J.D., Shokat, K.M., and Fisher, R.P. (2006). Dichotomous but stringent

substrate selection by the dual-function Cdk7 complex revealed by chemical genetics. *Nat. Struct. Mol. Biol.* **13**, 55–62.

Lavigne, M.D., Konstantopoulos, D., Ntakou-Zamplara, K.Z., Liakos, A., and Foustier, M. (2017). Global unleashing of transcription elongation waves in response to genotoxic stress restricts somatic mutation rate. *Nat. Commun.* **8**, 2076.

Li, H., Handsaker, B., Wysoker, A., Fennell, T., Ruan, J., Homer, N., Marth, G., Abecasis, G., and Durbin, R.; 1000 Genome Project Data Processing Subgroup (2009). The Sequence Alignment/Map format and SAMtools. *Bioinformatics* **25**, 2078–2079.

Lin, C., Smith, E.R., Takahashi, H., Lai, K.C., Martin-Brown, S., Florens, L., Washburn, M.P., Conaway, J.W., Conaway, R.C., and Shilatifard, A. (2010). AFF4, a component of the ELL/P-TEFb elongation complex and a shared subunit of MLL chimeras, can link transcription elongation to leukemia. *Mol. Cell* **37**, 429–437.

Lindsey-Boltz, L.A., and Sancar, A. (2007). RNA polymerase: the most specific damage recognition protein in cellular responses to DNA damage? *Proc. Natl. Acad. Sci. USA* **104**, 13213–13214.

Liu, P., Xiang, Y., Fujinaga, K., Bartholomeeusen, K., Nilson, K.A., Price, D.H., and Peterlin, B.M. (2014). Release of positive transcription elongation factor b (P-TEFb) from 7SK small nuclear ribonucleoprotein (snRNP) activates hexamethylene bisacetamide-inducible protein (HEXIM1) transcription. *J. Biol. Chem.* **289**, 9918–9925.

Luo, Z., Lin, C., and Shilatifard, A. (2012). The super elongation complex (SEC) family in transcriptional control. *Nat. Rev. Mol. Cell Biol.* **13**, 543–547.

McKay, B.C., Stubbert, L.J., Fowler, C.C., Smith, J.M., Cardamore, R.A., and Spronck, J.C. (2004). Regulation of ultraviolet light-induced gene expression by gene size. *Proc. Natl. Acad. Sci. USA* **101**, 6582–6586.

McNamara, R.P., McCann, J.L., Gudipaty, S.A., and D'Orso, I. (2013). Transcription factors mediate the enzymatic disassembly of promoter-bound 7SK snRNP to locally recruit P-TEFb for transcription elongation. *Cell Rep.* **5**, 1256–1268.

McNamara, R.P., Reeder, J.E., McMillan, E.A., Bacon, C.W., McCann, J.L., and D'Orso, I. (2016). KAP1 Recruitment of the 7SK snRNP Complex to Promoters Enables Transcription Elongation by RNA Polymerase II. *Mol. Cell* **61**, 39–53.

Michels, A.A., Fraldi, A., Li, Q., Adamson, T.E., Bonnet, F., Nguyen, V.T., Sedore, S.C., Price, J.P., Price, D.H., Lania, L., and Bensaude, O. (2004). Binding of the 7SK snRNA turns the HEXIM1 protein into a P-TEFb (CDK9/cyclin T) inhibitor. *EMBO J.* **23**, 2608–2619.

Mumbach, M.R., Granja, J.M., Flynn, R.A., Roake, C.M., Satpathy, A.T., Rubin, A.J., Qi, Y., Jiang, Z., Shams, S., Louie, B.H., et al. (2019). HiChIRP reveals RNA-associated chromosome conformation. *Nat. Methods* **16**, 489–492.

Muñoz, M.J., Pérez Santangelo, M.S., Paronetto, M.P., de la Mata, M., Pelisch, F., Boireau, S., Glover-Cutter, K., Ben-Dov, C., Blaustein, M., Lozano, J.J., et al. (2009). DNA damage regulates alternative splicing through inhibition of RNA polymerase II elongation. *Cell* **137**, 708–720.

Nguyen, V.T., Kiss, T., Michels, A.A., and Bensaude, O. (2001). 7SK small nuclear RNA binds to and inhibits the activity of CDK9/cyclin T complexes. *Nature* **414**, 322–325.

Nojima, T., Gomes, T., Grosso, A.R.F., Kimura, H., Dye, M.J., Dhir, S., Carmo-Fonseca, M., and Proudfoot, N.J. (2015). Mammalian NET-Seq Reveals Genome-wide Nascent Transcription Coupled to RNA Processing. *Cell* **161**, 526–540.

Nojima, T., Gomes, T., Carmo-Fonseca, M., and Proudfoot, N.J. (2016). Mammalian NET-seq analysis defines nascent RNA profiles and associated RNA processing genome-wide. *Nat. Protoc.* **11**, 413–428.

Nojima, T., Tellier, M., Foxwell, J., Ribeiro de Almeida, C., Tan-Wong, S.M., Dhir, S., Dujardin, G., Dhir, A., Murphy, S., and Proudfoot, N.J. (2018). Deregulated Expression of Mammalian lncRNA through Loss of SPT6 Induces R-Loop Formation, Replication Stress, and Cellular Senescence. *Mol. Cell* **72**, 970–984.e7.

Parua, P.K., Booth, G.T., Sansó, M., Benjamin, B., Tanny, J.C., Lis, J.T., and Fisher, R.P. (2018). A Cdk9-PP1 switch regulates the elongation-termination transition of RNA polymerase II. *Nature* **558**, 460–464.

Patro, R., Duggal, G., Love, M.I., Irizarry, R.A., and Kingsford, C. (2017). Salmon provides fast and bias-aware quantification of transcript expression. *Nat. Methods* **14**, 417–419.

Peterlin, B.M., and Price, D.H. (2006). Controlling the elongation phase of transcription with P-TEFb. *Mol. Cell* **23**, 297–305.

Price, D.H. (2000). P-TEFb, a cyclin-dependent kinase controlling elongation by RNA polymerase II. *Mol. Cell. Biol.* **20**, 2629–2634.

Quaresma, A.J.C., Bugai, A., and Barboric, M. (2016). Cracking the control of RNA polymerase II elongation by 7SK snRNP and P-TEFb. *Nucleic Acids Res.* **44**, 7527–7539.

Ramírez, F., Ryan, D.P., Grüning, B., Bhardwaj, V., Kilpert, F., Richter, A.S., Heyne, S., Dündar, F., and Manke, T. (2016). deepTools2: a next generation web server for deep-sequencing data analysis. *Nucleic Acids Res.* **44** (W1), W160–W165.

Rodríguez-Castañeda, F., Lemma, R.B., Cuervo, I., Bengtsen, M., Moen, L.M., Ledsaak, M., Eskeland, R., and Gabrielsen, O.S. (2018). The SUMO protease SENP1 and the chromatin remodeler CHD3 interact and jointly affect chromatin accessibility and gene expression. *J. Biol. Chem.* **293**, 15439–15454.

Sansó, M., Levin, R.S., Lipp, J.J., Wang, V.Y., Greifenberg, A.K., Quezada, E.M., Ali, A., Ghosh, A., Larochelle, S., Rana, T.M., et al. (2016). P-TEFb regulation of transcription termination factor Xrn2 revealed by a chemical genetic screen for Cdk9 substrates. *Genes Dev.* **30**, 117–131.

Smith, E., and Shilatifard, A. (2013). Transcriptional elongation checkpoint control in development and disease. *Genes Dev.* **27**, 1079–1088.

Sobhian, B., Laguet, N., Yatim, A., Nakamura, M., Levy, Y., Kiernan, R., and Benkirane, M. (2010). HIV-1 Tat assembles a multifunctional transcription elongation complex and stably associates with the 7SK snRNP. *Mol. Cell* **38**, 439–451.

Soneson, C., Yao, Y., Bratus-Neuenschwander, A., Patrignani, A., Robinson, M.D., and Hussain, S. (2019). A comprehensive examination of Nanopore native RNA sequencing for characterization of complex transcriptomes. *Nat. Commun.* **10**, 3359.

Tufegdžić Vidaković, A., Mitter, R., Kelly, G.P., Neumann, M., Harreman, M., Rodríguez-Martínez, M., Herlihy, A., Weems, J.C., Boeing, S., Encheva, V., et al. (2020). Regulation of the RNAPII Pool Is Integral to the DNA Damage Response. *Cell* **180**, 1245–1261.e21.

Van Herreweghe, E., Egloff, S., Goiffon, I., Jady, B.E., Froment, C., Monsarrat, B., and Kiss, T. (2007). Dynamic remodelling of human 7SK snRNP controls the nuclear level of active P-TEFb. *EMBO J.* **26**, 3570–3580.

Vos, S.M., Farnung, L., Boehning, M., Wigge, C., Linden, A., Urlaub, H., and Cramer, P. (2018). Structure of activated transcription complex Pol II-DSIF-PAF-SPT6. *Nature* **560**, 607–612.

Williams, L.H., Fromm, G., Gokey, N.G., Henriques, T., Muse, G.W., Burkholder, A., Fargo, D.C., Hu, G., and Adelman, K. (2015). Pausing of RNA polymerase II regulates mammalian developmental potential through control of signaling networks. *Mol. Cell* **58**, 311–322.

Williamson, L., Saponaro, M., Boeing, S., East, P., Mitter, R., Kantidakis, T., Kelly, G.P., Lobley, A., Walker, J., Spencer-Dene, B., et al. (2017). UV Irradiation Induces a Non-coding RNA that Functionally Opposes the Protein Encoded by the Same Gene. *Cell* **168**, 843–855.e13.

Xue, Y., Yang, Z., Chen, R., and Zhou, Q. (2010). A capping-independent function of MePCE in stabilizing 7SK snRNA and facilitating the assembly of 7SK snRNP. *Nucleic Acids Res.* **38**, 360–369.

Yamada, T., Yamaguchi, Y., Inukai, N., Okamoto, S., Mura, T., and Handa, H. (2006). P-TEFb-mediated phosphorylation of hSpt5 C-terminal repeats is critical for processive transcription elongation. *Mol. Cell* **21**, 227–237.

Yang, Z., Zhu, Q., Luo, K., and Zhou, Q. (2001). The 7SK small nuclear RNA inhibits the CDK9/cyclin T1 kinase to control transcription. *Nature* **414**, 317–322.

Yang, Z., Yik, J.H., Chen, R., He, N., Jang, M.K., Ozato, K., and Zhou, Q. (2005). Recruitment of P-TEFb for stimulation of transcriptional elongation by the bromodomain protein Brd4. *Mol. Cell* 19, 535–545.

Yokoyama, A., Lin, M., Naresh, A., Kitabayashi, I., and Cleary, M.L. (2010). A higher-order complex containing AF4 and ENL family proteins with P-TEFb facilitates oncogenic and physiologic MLL-dependent transcription. *Cancer Cell* 17, 198–212.

Yu, M., Yang, W., Ni, T., Tang, Z., Nakadai, T., Zhu, J., and Roeder, R.G. (2015). RNA polymerase II-associated factor 1 regulates the release and phosphorylation of paused RNA polymerase II. *Science* 350, 1383–1386.

Zhou, Q., and Yik, J.H. (2006). The Yin and Yang of P-TEFb regulation: implications for human immunodeficiency virus gene expression and global control of cell growth and differentiation. *Microbiol. Mol. Biol. Rev.* 70, 646–659.

Zhou, Q., Li, T., and Price, D.H. (2012). RNA polymerase II elongation control. *Annu. Rev. Biochem.* 81, 119–143.

STAR★METHODS

KEY RESOURCES TABLE

REAGENT or RESOURCE	SOURCE	IDENTIFIER
Antibodies		
Mouse monoclonal anti-RNA polymerase II CTD (used in mNET-seq)	MBL Life Science	Cat# MABI0601; RRID:AB_2728735
Rabbit polyclonal anti-RNA polymerase II (used in ChIP)	Bethyl Laboratories	Cat# 304-405A; RRID:AB_2620600
Rabbit monoclonal anti-CDK9 (clone C12F7) (used in Western Blot)	Cell Signaling Technology	Cat# 2316; RRID:AB_2291505
Mouse monoclonal anti-CDK9 (used in ChIP)	Santa Cruz Biotechnology	Cat# sc-13130; RRID:AB_627245
Rabbit polyclonal anti-Cyclin T1 (use in IP)	Abcam	Cat# ab2098; RRID:AB_302836
Mouse monoclonal anti-Cyclin T1 (used in Western Blot)	Santa Cruz Biotechnology	Cat# sc-271348; RRID:AB_10608086
Rabbit polyclonal anti-AFF4	Bethyl Laboratories	Cat# A302-539A; RRID:AB_1998983
Mouse monoclonal anti-SPT5	Santa Cruz Biotechnology	Cat# sc-133217; RRID:AB_2196394
Rabbit polyclonal anti-SPT6	Novus Biologicals	Cat# NB100-2582; RRID:AB_2196402
Rabbit polyclonal anti-Histone H3	Abcam	Cat# ab1791; RRID:AB_302613
Rabbit polyclonal anti-NELFE	Sigma-Aldrich	Cat# HPA007187; RRID:AB_1856161
Rabbit polyclonal anti-HEXIM1	Abcam	Cat# ab25388; RRID:AB_2233058
Rabbit polyclonal anti-LARP7	Abcam	Cat# ab134746
Rabbit polyclonal anti-MEPCE	Abcam	Cat# ab185991
Mouse monoclonal anti-hnRNP A1 (clone 4B10)	Santa Cruz Biotechnology	Cat# sc-32301; RRID:AB_627729
Mouse monoclonal anti-GAPDH	Millipore	Cat# MAB374; RRID:AB_2107445
Rabbit polyclonal anti-GST	Sigma-Aldrich	Cat# G7781; RRID:AB_259965
Rabbit polyclonal anti-PAF1	Abcam	Cat# ab137519
Rat monoclonal anti-Ser2P (clone 3E10)	Active Motif	Cat# 61083; RRID:AB_2687450
Rat monoclonal anti-Ser5P (clone 3E8)	Active Motif	Cat# 61085; RRID:AB_2687451
Rat monoclonal anti-Ser7P (clone 4E12)	Active Motif	Cat# 61087; RRID:AB_2687452
Goat polyclonal anti-Rabbit IgG (H+L), HRP Conjugate antibody	Promega	Cat# W4011; RRID:AB_430833
Goat polyclonal anti-Mouse IgG (H+L), HRP Conjugate antibody	Promega	Cat# W4021; RRID:AB_430834
Bacterial strains		
<i>E. coli</i> DH5 alpha	Lab strain	N/A
Chemicals, peptides, and recombinant proteins		
GST-Spt5 CTR1	Sansó et al., 2016	N/A
Puromycin dihydrochloride	Sigma-Aldrich	Cat# P8833
T4 polynucleotide kinase (PNK), 3' phosphatase minus	NEB	Cat# M0236S
T4 RNA ligase, deletion mutant 2	Epicenter	Cat# LR2D1132K
SuperScript III reverse transcriptase	ThermoFischer Scientific	Cat# 18080044
Novex 6% TBE gel, 10 well	ThermoFischer Scientific	Cat# EC6265BOX
Novex 6% TBE-Urea (TBU) gel, 10 well	ThermoFischer Scientific	Cat# EC6865BOX
Critical commercial assays		
TruSeq small RNA library preparation kit	Illumina	Cat# RS-200-0012
Dynabeads M280 sheep anti-mouse IgG	Invitrogen	Cat# 11202D

(Continued on next page)

Continued

REAGENT or RESOURCE	SOURCE	IDENTIFIER
Dynabeads MyOne Streptavidin C1	Invitrogen	Cat# 65002
Click-iT® RNA Imaging kit	Invitrogen	Cat# C10329

Deposited data

Raw and processed NGS data (mNET-seq, ChIRP-seq)	This paper	GEO:GSE147055
HAP1 RNA-seq	Soneson et al., 2019	ArrayExpress: E-MTAB-7757
HAP1 RNA-seq	Rodríguez-Castañeda et al., 2018	GEO: GSE111272
Source data from Figures 1, 3, and 6 (Mendeley dataset)	https://dx.doi.org/10.17632/2fb8nxxn6ft.1	N/A

Cell lines

Human HAP1 cells	Horizon discovery	Cat# C859
Human 7SK KO cells	This paper	N/A
Human LARP7 KO cells	This paper	N/A
Human 7SKex KO cells	This paper	N/A

Oligonucleotides

siGENOME Human LARP7 siRNA SMARTpool	Dharmacon	M-020996-01-0010
Primers for Northern blot	This paper	Table S1
Primers for qRT-PCR and qPCR	This paper	Table S1
Primers for CRISPR/Cas9 guide-RNAs	This paper	Table S1
Biotinylated oligonucleotides for 7SK ChIRP	This paper	Table S1

Plasmids

Plasmid: pSpCas9(BB)-2A-Puro (PX459) V2.0	Addgene	Cat# 62988
Plasmids: PX459-7SK guides	This paper	N/A
Plasmid: PX459-LARP7 guide	This paper	N/A

Softwares and algorithms

Cutadapt version 1.13	https://cutadapt.readthedocs.io/en/stable/installation.html	N/A
STAR version 2.6.1d	https://github.com/alexdobin/STAR	N/A
SAMtools version 1.3.1	http://www.htslib.org/	N/A
deepTools2 version 2.5.0.1	https://deeptools.readthedocs.io/en/latest/index.html	N/A
Picardtools	http://broadinstitute.github.io/picard/	N/A
Salmon (version 0.13.1)	https://combine-lab.github.io/salmon/	N/A

RESOURCE AVAILABILITY

Lead contact

Further information and requests for resources and reagents should be directed to and will be fulfilled by Sylvain Egloff (sylvain.egloff@univ-tlse3.fr).

Materials availability

The 7SK and Larp7 KO cell lines generated in this study are available from the Lead Contact without restriction.

Data and code availability

The datasets produced in this study are available in the following databases: *mNET-Seq* and *ChIRP-seq* data: Gene Expression Omnibus GSE147055. Source data for [Figures 1A–1C](#), [1E](#), [3A](#), [6D](#), and [6E](#) were deposited on Mendeley at: <https://dx.doi.org/10.17632/2fb8nxxn6ft.1>.

EXPERIMENTAL MODEL AND SUBJECT DETAILS

The knock-out cell lines generated in this study were derived from human HAP1 parental cells (purchased from Horizon discovery). The cells were routinely tested for the presence of mycoplasma using MycoAlert (Lonza).

METHOD DETAILS

General procedures

DNA, RNA and protein manipulations were performed according to standard laboratory procedures. Oligonucleotide sequences (Eurofins MWG Operon) are listed in [Table S1](#). Human HAP1 cells were grown in Iscove's Modified Dulbecco's Medium (IMDM) supplemented with 10% (v/v) fetal bovine serum, 1 mM sodium pyruvate and 100 μ g/ml of penicillin and streptomycin (GIBCO, Invitrogen).

UV irradiation

Unless stated otherwise, cells were irradiated with UV-C light (254 nm, 40 J/m²) with Stratalinker (Fischer Bioblock Scientific). Before UV irradiation, the medium was replaced with PBS, and the cells were irradiated from above with lids off from 16 cm distance. The actual UV dose received by cells was confirmed with a VLX-254 radiometer (Vilbert-Lourmat).

Cell proliferation assays

Human HAP1, 7SK KO and 7SK RST cells (about 4×10^5) were seeded in 10 cm plates and at each point in time (1, 2, 3 and 4 days), they were counted with a Beckman Coulter Z2 particle counter in quadruplicate. For monitoring growth recovery after UV-induced DNA damage, cells were irradiated with lower dose of UV (10 J/m²). Four independent proliferation assays were performed for each cell line. MTS proliferation assay were performed using the CellTiter 96 AQueous One Solution cell Proliferation Assay (Promega, G3581) according to the manufacturer's instructions. About 5×10^3 cells/well were seeded in 96-well plates. After 1, 2, 3 and 4 days of incubation, 20 μ L of MTS reagent was added to each well and further incubated for 1 h at 37°C. The absorbance at 490 nm was measured with a colorimetric plate reader.

Clonogenic assays

HAP1, 7SK KO and Larp7 KO cells were seeded at a clonal density (about 1×10^3) in 10 cm diameter dishes, and irradiated 12 h later with moderate dose of UV (10 J/m²). 10 days after irradiation, cells were stained with crystal violet (Sigma) and colonies were counted. Non-irradiated cells were used as a seeding control for calculation of the surviving fraction.

EU incorporation assays

Cells were incubated in IMDM supplemented with 0.5 mM 5-ethynyluridine (EU) for 1 hr, washed with cold PBS, fixed with 3.7% formaldehyde and permeabilized with 0.5% Triton 100X. EU incorporation was revealed with Click-IT® RNA Imaging kit (Invitrogen) using Alexa Fluor® 488 dye and Hoechst 33342 according to manufacturer's instructions. Coverslips were mounted in Vectashield medium. The mean EU fluorescence intensity per cell was obtained using ImageJ software by averaging the mean gray value of the EU signal measured in each nucleus.

Inactivation of 7SK and LARP7 genes by CRISPR/Cas9

To generate synthetic DNA encoding appropriately designed sgRNAs, 5'-terminally phosphorylated overlapping oligodeoxynucleotides were annealed and inserted into the *Bbs*I site of pSpCas9(BB)-2A-Puro (PX459) V2.0 by overnight incubation with T4 DNA ligase (NEB) at room temperature. The resulting pX459/sgRNA expression vectors were transfected into HAP1 cells with Lipofectamine 2000 (Invitrogen) according to the manufacturer's instructions. Two days after transfection, cells were transferred into puromycin-containing (2 μ g/ml) selective medium and grown for additional 48 h before establishment of monoclonal stable cell lines by limited dilution under non-selective conditions. 7SK and Larp7 expression was monitored by northern and western blot analyses, respectively. The targeted genomic fragments were PCR-amplified and analyzed by DNA sequencing.

Glycerol gradient analysis

Cells were collected on ice and lysed in 10 mM HEPES, 150 mM NaCl, 2 mM MgCl₂, 1 mM EDTA, 1 mM DTT, 0.1% Nonidet P-40, complemented with PMSF (0.5 mM) and 1 x cComplete EDTA-free protease inhibitor cocktail (Roche) and disrupted by sonication five times for 30 s with 30 s intervals with a Bioruptor Plus Sonicator (Diagenode) at high setting. After centrifugation at 12,000 x g for 10 min, the soluble extracts were loaded onto 10%–40% glycerol gradients made in 10 mM HEPES, 150 mM NaCl, 2 mM MgCl₂, 1 mM EDTA, 1 mM DTT supplemented with PMSF and protease inhibitor cocktail and centrifuged for 16 h at 41,000 rpm in a Beckman SW41 rotor.

siRNA-mediated Larp7 knockdown

Control and Larp7 mRNA-targeting siRNAs were purchased from Dharmacon. The siRNAs were introduced into HAP1 cells by two subsequent electroporation reactions at 0 and 48 h and the transfected cells were incubated for additional 24 h before analysis.

Chromatin fractionation

About 8×10^6 cells were washed in ice-cold PBS (phosphate buffered saline, pH 7.3) and lysed in 4 mL of HLB/NP-40 buffer containing 10 mM Tris-HCl, pH 7.5, 10 mM NaCl, 2.5 mM $MgCl_2$ and 0.5% Nonidet P-40 by incubation on ice for 5 min. The lysate was layered over 1 mL of 10% sucrose cushion made in HLB/NP-40 buffer and intact nuclei were collected by centrifugation at $420 \times g$ for 5 min at $4^\circ C$. The nuclear pellet was resuspended in 125 μL of 20 mM Tris-HCl, pH 8.0, 75 mM NaCl, 0.5 mM EDTA, 50% glycerol and 1 x cOmplete protease inhibitor cocktail (Roche). To lyse nuclei, 1.2 mL of 20 mM HEPES-KOH, pH 7.6, 7.5 mM $MgCl_2$, 0.2 mM EDTA, 300 mM NaCl, 1% Nonidet P-40 and 1 M Urea, supplemented with 1 x cOmplete protease and 1 x PhosStop phosphatase inhibitors (Roche) was added. The mixture was incubated on ice for 15 min with vigorous vortex agitations for 5 s in every 3 min. Chromatin was pelleted by centrifugation at $10,000 \times g$ for 10 min at $4^\circ C$, resuspended in 500 μL NET-2 buffer (50 mM Tris-HCl, pH 7.5, 200 mM NaCl and 0.1% Nonidet P-40) and solubilized by sonication (3×10 s) with a Bioruptor Plus sonifier equipped with a microtip (setting high). The chromatin extract was clarified by centrifugation at $10,000 \times g$ for 10 min before SDS-PAGE analysis.

Immunoprecipitation and protein analysis

HAP1 cells were collected, washed in ice-cold PBS, resuspended in 0.5 mL of cold NET-2 buffer and disrupted with a Bioruptor Plus Sonicator by sonication five times for 30 s with 30 s intervals at high setting. Cell debris were removed by sedimentation at $16,000 \times g$ for 10 min and the clarified extracts were reacted with 2 μg of antibodies coupled to 20 μL of packed protein A agarose beads (Sigma). After immunoprecipitation, beads were washed six times in NET-2 buffer and the associated proteins were eluted with 1 x SDS-PAGE loading buffer.

Chromatin immunoprecipitation

Formaldehyde cross-linking and IP of chromatin was performed essentially as described previously (Egloff et al., 2017). HAP1 cells were cross-linked with 1% formaldehyde for 10 min at RT and quenched for 5 min after adding glycine at 125 mM final concentration. Cells were resuspended in cell lysis buffer (5 mM PIPES, pH 8.0, 85 mM KCl, 0.5% Nonidet P-40 supplemented with 1 x protease inhibitor cocktail) and incubated on ice for 10 min. After collection by centrifugation at $2,300 \times g$ for 5 min, nuclei were lysed in nuclei lysis buffer (50 mM Tris-HCl, pH 8.1, 10 mM EDTA, 1% SDS) for 20 min. Chromatin was disrupted with a Bioruptor Plus sonifier (high power setting, 20 cycles for 30 s on and 30 s off) on ice. The extract was cleared by centrifugation and incubated with 2 μg of appropriate antibody overnight at $4^\circ C$. Immunocomplexes were immobilized by reacting with 10 μL of BSA-saturated Pansorbin cells (Calbiochem) for 15 min at $4^\circ C$. After extensive and stringent washing and elution, protein-DNA cross-links were reversed by incubation at $67^\circ C$ for 5 h and DNA was deproteinized with proteinase K treatment at $50^\circ C$ for 30 min. DNA was purified by the Nucleospin PCR cleanup kit of Macherey-Nagel. ChIP samples were directly analyzed by qPCR.

Mammalian native elongating transcript sequencing (mNET-seq)

mNET-seq was carried out essentially as described earlier (Nojima et al., 2016). In brief, the chromatin fraction was isolated from about 10^7 HAP1 cells. Chromatin was digested in 100 μL of micrococcal nuclease (MNase) reaction buffer containing 40 units/ μL of MNase for 2 min at $37^\circ C$ in a thermomixer (1,400 rpm). After inactivation of MNase with 10 μL of 25 mM EGTA, the reaction mixture was clarified by centrifugation at $10,000 \times g$ for 5 min. The supernatant was diluted with 400 μL of NET-2 buffer and RNAPII antibody-conjugated beads were added. For each mNET-seq reaction, 10 μg of RNAPII antibody was used and immunoprecipitation was performed at $4^\circ C$ for 1 h. The beads were washed six times with 1 mL of NET-2 buffer and once with 100 μL of 1 x PNKT buffer (1 x PNKT supplemented with 0.05% Triton X-100). The washed beads were incubated in 50 μL PNK reaction mix (1 x PNKT supplemented with 1 mM ATP and 0.05 U/ml T4 polynucleotide kinase 3' phosphatase minus (NEB) in a Thermomixer (1,400 rpm) at $37^\circ C$ for 6 min. Beads were washed with 1 mL of NET-2 buffer and RNA was extracted with Trizol reagent, precipitated with ethanol and dissolved in urea loading buffer containing 7M Urea, 1xTBE, 0.1% bromophenol blue (BPB) and 0.1% xylene cyanol (XC). RNA was size-fractionated on a 6% TBE-urea gel (Invitrogen) at 200 V for 5 min. To select 30-160 nt-long RNAs, the gel fragment between BPB and XC was excised and placed into a 0.5 mL microtube carrying 3-4 small holes made with a 25G needle at its bottom. The microtube with the gel slice was placed into a 1.5 mL tube and centrifuged at 12,000 rpm for 1 min. Small RNAs were eluted from gel with RNA elution buffer (1 M NaOAc and 1 mM EDTA) at $25^\circ C$ for 1 h in Thermomixer (900 rpm). Gel debris were eliminated by centrifugation through a SpinX column (Coster) equipped with two glass filters (Millipore) and RNA was ethanol-precipitated from the flow-through. mNET-seq libraries were prepared with the TruSeq small RNA library preparation kit (Illumina, cat. no. RS-200-0012) using T4 RNA ligase (Epicenter, cat. no. LR2D1132K), following instructions of the TruSeq manual of Illumina. 14 cycles of PCR were applied to amplify the library. Before sequencing, the amplified DNA libraries were size-selected on a 6% TBE gel to select 150-230 bp-long PCR products and to exclude primer-primer ligated DNAs. DNA extraction from the gel was performed as described above. Deep sequencing (HiSeq4000, Illumina) was conducted at the Wellcome Trust Centre for Human Genetics (WTCHG), Oxford.

Chromatin isolation by RNA purification (ChIRP) and deep sequencing

Chromatin isolation by RNA purification experiments were performed essentially as described earlier (Chu et al., 2012). Briefly, HAP1 cells ($\sim 10 \times 10^7$) were harvested and cross-linked in PBS containing 1% of glutaraldehyde with continuous gentle agitation for 10 min at RT. The reaction was stopped by adding glycine to 125 mM final concentration. Cells were collected, washed with PBS, resuspended in lysis buffer (50 mM Tris-HCl, pH 7.0, 10 mM EDTA, 1% SDS and protease inhibitors) and sonicated for 2 h at 4°C (Bioruptor Plus, Diagenode, 30 s pulses with 30 s intervals at high setting). Hybridization of 7SK-specific and control biotinylated oligonucleotides (~ 100 pmol/ml of chromatin extract) to cellular RNAs was performed in 50 mM Tris-HCl, pH 7.0, 750 mM NaCl, 1% SDS, 1 mM EDTA, 15% formamide and protease inhibitors at 37°C for 4 h. Biotinylated oligonucleotides were affinity-selected by Streptavidin magnetic beads (Dynabeads MyOne Streptavidin C1, 65002, Invitrogen) for 30 min at RT. Beads were extensively washed in 2 × SSC, 0.5% SDS supplemented with protease inhibitors, and the bound chromatin was eluted in DNA elution buffer (50 mM NaHCO₃, 1% SDS). DNA was deproteinized with proteinase K treatment and purified by the Nucleospin PCR cleanup kit of Macherey-Nagel. DNA deep sequencing was performed as described above.

mNET-seq data processing

mNET-seq data were processed as previously described (Nojima et al., 2018). Adapters were trimmed with Cutadapt in paired-end mode with the following parameters: -q 15, 10–minimum-length 10 -a TGAATTCTCGGGTGCCAAGG -A GATCGTCGGACTGTGA GAACCTGAAC. Trimmed reads were mapped to the human hg38 reference sequence with STAR (Dobin et al., 2013) at parameters:–runThreadN 16–genomeLoad LoadAndKeep–readFilesCommand gunzip -c -k–limitBAMsortRAM 20000000000–outSAMtype BAM SortedByCoordinate. SAMtools (Li et al., 2009) was used to retain only properly paired and mapped reads (–f 3). A custom python script (Nojima et al., 2015, 2016) was used to obtain the 3' nucleotide of the second read and the strandedness of the first read. Strand-specific bam files were generated with SAMtools (–f 97 and –f 81). FPKM normalized bigwig files were generated for each bam files with deepTools2 (Ramírez et al., 2016) bamCoverage tool (–bs 1 –p max –normalizeUsingRPKM).

ChIRP-seq data processing

Adapters were trimmed with Cutadapt in paired-end mode with the following parameters: -q 15, 10–minimum-length 10 -A AGATCG GAAGAGCGTCGTGTAGGGAAGAGTGTAGATCTCGGTGGTGCCTGATCATT -a AGATCGGAAGAGCACACGTCTGAACTCCAGT CAC. Trimmed reads were mapped to the human hg38 reference genome with STAR and at parameters:

```
–runThreadN 16–genomeLoad LoadAndKeep–readFilesCommand gunzip -c -k–alignIntronMax 1–limitBAMsortRAM 20000000000–outSAMtype BAM SortedByCoordinate. Properly paired and mapped reads were filtered with SAMtools (–f 3). PCR duplicates were removed with Picard MarkDuplicates tool. FPKM normalized bigwig files were generated for each bam files with deepTools2 bamCoverage tool (–bs 10 –p max –normalizeUsingRPKM –e).
```

RNA-seq data processing

HAP1 poly(A)⁺ RNA-seq were retrieved from Soneson et al. (2019), ArrayExpress number E-MTAB-7757. Adapters were trimmed with Cutadapt in paired-end mode with the following parameters:–minimum-length 10 -q 15,10 -a AGATCGGAAGAGCACACGTCT GAACTCCAGTCA -A AGATCGGAAGAGCGTCGTGTAGGGAAGAGTGT. Trimmed reads were mapped to the human hg38 reference sequence with STAR and the parameters:

```
–runThreadN 16–genomeLoad LoadAndKeep–readFilesCommand gunzip -c -k–limitBAMsortRAM 20000000000–quantMode TranscriptomeSAM GeneCounts–outSAMtype BAM SortedByCoordinate. SAMtools was used to retain only properly paired and mapped reads (–f 3). Quantification of the different mRNA isoforms from the RNA-seq data was performed with salmon version 0.13.1 (Patro et al., 2017) and the salmon quant command.
```

Transcription unit (TU) definition

Gencode V29 annotation, based on the hg38 version of the human genome, was used to extract TUs. For each protein-coding gene, we defined the start and end sites as the TSS and the poly(A) site from the most expressed mRNA isoform defined in the HAP1 RNA-seq data. For meta-analyses, only non-overlapping protein-coding genes (with a 2.5 kb-free window before TSS and after poly(A) site) with a TU > 2 kb and RNA-seq signal > 0 were analyzed. lncRNAs were taken from the Gencode V29 annotation. PROMPTS were taken from Chen et al. (2016). The eRNAs were taken from the PrESSTo database, which is part of the FANTOM5 project.

Reads quantification

Total read base count for mNET-seq data were computed with samtools bedcov tool using strand-specific bam files and normalized to 100 million paired-end reads and to the region's length. Only the regions with a positive signal in UV- or UV+ were kept. For the samples having a signal ≤ 0 on the remaining regions, their values were put to the minimal value divided by two. Spearman correlations were calculated with deepTools multiBamSummary tool with default options followed by the plotCorrelation tool with the following options: -c spearman–skipZeros–log1p–xRange 0 15–yRange 0 15.

Metagene profiles

Metagene profiles were generated with deepTools2 computeMatrix tool with a bin size of 10 bp and the plotting data obtained with plotProfile -outFileNameData tool. Graphs representing the ChIRP-seq signal or the mNET-seq signal were then created with GraphPad Prism 8.1.1.

Fluorescence *in situ* hybridization

Fluorescence *in situ* hybridization, image acquisition, and processing have been described (Darzacq et al., 2002). The following oligonucleotide probe was used to detect HAP1 7SK snRNA: (5'-G*TGTCCTGGAGTCTTGAAGC*-3'). The aminoallyl-nucleotides labeled with FluorLink Cy3 monofunctional reactive dye (GE Healthcare) are indicated by asterisks. Nuclear DNA was visualized with 1 μ g/ml DAPI.

RNA analysis

RNAs from HAP1 cells, cell extracts and protein A agarose beads were purified by the guanidine thiocyanate/phenol-chloroform RNA extraction procedure. For Northern blot analyses, RNAs were size-fractionated on 6% sequencing gels, electroblotted onto Hybond-N nylon membrane and probed with 5'-³²P-labeled oligonucleotides. Real-time quantitative RT-PCR was performed on 2 μ g of total RNA. DNA first strands were synthesized by GoScript reverse transcriptase (Promega), and qPCR reactions were performed on a BioRad C1000 Touch thermal cycler using the iQ SYBR Green Supermix of BioRad. The delta-delta Ct method was used for relative quantification of RNA accumulation.

In vitro kinase assay

Cell extracts were prepared in NET-2 buffer as described for IP assays and their protein concentration was determined by the Bradford method. Indicated amounts of cell extracts were incubated with 1 μ g of GST-fused Spt5 CTR1 substrate (provided by Dr R.P. Fisher) in 10 mM HEPES, pH 7.9, 150 mM NaCl, 1 mM DTT, 10 mM MgCl₂, 100 μ M unlabeled ATP and [γ -³²P]ATP (10 μ Ci, 3,000 Ci/mmol) for 15 min at 30°C (Sansó et al., 2016). Reactions were stopped with EDTA at 20 mM final concentration and the reaction mixture was incubated with 20 μ L of Glutathione Sepharose beads (GE Healthcare) for 1 h. The beads were washed five times with NET-2 buffer and the bound GST-CTR1 was eluted with 1 \times SDS-PAGE loading buffer. After size-fractionation by SDS-PAGE, GST-CTR1 was electroblotted onto a Hybond-C nylon membrane. Phosphorylated GST-CTR1 was visualized by autoradiography and its phosphorylation level was determined by phosphorimager quantitation.

QUANTIFICATION AND STATISTICAL ANALYSIS

Statistical details of experiments can be found in the figure legends. Analysis was performed using either Excel, GraphPad Prism or R. Significance was assessed using Student's t test or Wilcoxon test. Values with a p value lower than 0.05 were considered statistically significant. Error bars represent standard deviation of at least three independent experiments.